Chem Soc Rev

TUTORIAL REVIEW

View Article Online
View Journal | View Issue

Cite this: *Chem. Soc. Rev.*, 2025, **54**, 601

Host molecules inside metal–organic frameworks: host@MOF and guest@host@MOF (Matrjoschka) materials†

Qiao Wu, [a] Jun Liang, *[ac] Dan Wang, [a] Ruihu Wang *[ac] and Christoph Janiak *[b]

The controllable encapsulation of host molecules (such as porphyrin, phthalocyanine, crown ether, calixarene or cucurbituril organic macrocycles, cages, metal–organic polyhedrons and enzymes) into the pores of metal–organic frameworks (MOFs) to form host-in-host (host@MOF) materials has attracted increasing research interest in various fields. These host@MOF materials combine the merits of MOFs as a host matrix and functional host molecules to exhibit synergistic functionalities for the formation of guest@host@MOF materials in sorption and separation, ion capture, catalysis, proton/ion conduction and biosensors. (This guest@host@MOF construction is reminiscent of Russian (Matrjoschka) dolls which are nested dolls of decreasing size placed one inside another.) In this tutorial review, the advantages of MOFs as a host matrix are presented; the encapsulation approaches and general important considerations for the preparation of host@MOF materials are introduced. The state-of-the-art examples of these materials based on different host molecules are shown, and representative applications and general characterization of these materials are discussed. This review will guide researchers attempting to design functional host@MOF and guest@host@MOF materials for various applications.

Received 24th August 2024

DOI: 10.1039/d4cs00371c

rsc.li/chem-soc-rev

Key learning points

1. Concepts of host@MOF and guest@host@MOF materials.
2. Encapsulation paths and important considerations for the fabrication of host@MOF materials.
3. Specific synthesis and general characterization techniques of various host@MOF materials.
4. Synergistic functionalities of host@MOF and guest@host@MOF materials.
5. Future opportunities and challenges in the field of MOF-encapsulated host molecules.

1. Introduction

Enzymes,[1,2] and artificial enzymes,[3–6] feature active sites and inherent cavities or pockets (as active domains) to selectively accommodate substrates and stabilize transition states, providing unique chemical environments to improve reaction efficiency and selectivity under mild conditions. Inspired by enzyme systems, many host molecules have been developed to show appealing ''host–guest recognition'' and ''interactions between molecules'' characteristics during the past decades,[7,8] giving birth to two generations of Nobel Prize Winners in 1987 and 2016.[9,10] Organic host molecules, such as cyclodextrins (CDs),[11] crown ethers (CEs),[12] calix[*n*]arenes (CAs),[13] cucurbit[*n*]urils (CBs),[14] pillar[*n*]arenes (PAs),[15] porphyrins (PPs),[16] and imine cages,[17] have tunable molecular structures and intrinsic pores (cavities) with unique host–guest properties, and have impacted various areas including recognition, sensing, biomimetic catalysis and smart materials. Hybrid host molecules like metal–organic polyhedrons (MOPs) are also of intense interest for their tunable structures and properties.[18] While great scientific progress has been made in the solution chemistry of enzymes and these host molecules, their solid chemistry as

[a] *School of Chemical Engineering and Technology, Hebei University of Technology, 300401 Tianjin, China. E-mail: jliang@hebut.edu.cn, ruihu@fjirsm.ac.cn*
[b] *Institut für Anorganische Chemie und Strukturchemie, Heinrich-Heine-Universität Düsseldorf, 40204 Düsseldorf, Germany. E-mail: janiak@uni-duesseldorf.de*
[c] *State Key Laboratory of Structural Chemistry, Fujian Institute of Research on the Structure of Matter, Chinese Academy of Sciences Fuzhou, Fujian 350002, China*

† Electronic supplementary information (ESI) available: Tables, abbreviations and additional figures. See DOI: https://doi.org/10.1039/d4cs00371c

functional materials is underdeveloped and has fuelled increasing interest of researchers in recent years.

These porous solid materials include: (i) covalent organic polymers (COPs) based on covalent bonds between host molecule monomers (such as CDs, PPs, cages);[19] (ii) metal–organic frameworks (MOFs) based on coordination bonds between host molecule linkers and metal nodes.[20] Some reviews of using host molecules as building blocks for porous materials, such as supramolecular organic frameworks,[21] MOFs,[22] COPs,[23] and covalent organic frameworks (COFs),[24] have been published. In addition to these reticular synthesis works by exploiting host molecules as building units, alternative methods are essential for relatively inert host molecules and delicate enzymes to obtain permanent porous materials.[25] There is increasing interest in fabricating MOF composites that consist of host entities encapsulated within the MOF pores. The enhanced performance of these host@MOF materials with respect to their constituents has also inspired the efforts of encapsulating enzymes and host molecules in MOFs.

There are no reviews of recent work on the encapsulation of various host molecules into MOFs to form host@MOF materials. We focus here on host@MOF materials with host molecules confined in MOFs (Fig. 1a), both of which can be further functionalized *via in situ* or post-synthetic modifications. Host@MOF materials may possess three kinds of domains: (i) the intrinsic pores or cavities of the host molecules, which can accommodate guest species (Fig. 1b); (ii) the formed extrinsic pores between host molecules and pore walls of the MOF; and (iii) the unoccupied native pores of the MOF (Fig. 1a). From a functional point of view, the intrinsic cavities can provide tunable recognition, adsorption and even catalytic sites; the extrinsic pores can provide selective mass transfer pathways to show interaction adsorption or repulsion effect; the unoccupied native pores together with the window

Qiao Wu

Qiao Wu received her PhD (2023) from Xiamen University under the joint supervision of Prof. Yuan-Biao Huang and Prof. Rong Cao of FJIRSM (Fujian Institute of Research on the Structure of Matter), Chinese Academy of Sciences. She subsequently works at Hebei University of Technology from 2023. Her current research interests mainly focus on porous crystalline materials for heterogeneous catalysis and energy conversion.

Jun Liang

Jun Liang received his MS (2014) under the supervision of Prof. Xin-Long Wang and Prof. Zhong-Min Su from NENU (Northeast Normal University), and his PhD (2018) under the supervision of Prof. Rong Cao and Prof. Yuan-Biao Huang from Xiamen University and FJIRSM (Fujian Institute of Research on the Structure of Matter), Chinese Academy of Sciences. He worked as a postdoctoral fellow with Prof. Christoph Janiak (Heinrich-Heine-Universität (HHU) Düsseldorf, Germany) from 2018 to 2021. His research interests focus on porous crystalline materials (MOFs, COFs), inorganic–organic hybrid materials for heterogeneous catalysis and environmental applications.

Dan Wang

Dan Wang received her PhD (2022) under the supervision of Prof. Zhong-Min Su at Changchun University of Science and Technology (CUST). She subsequently worked as a postdoctoral fellow with Prof. Ruihu Wang at the Hebei University of Technology from 2022. Her research interests focus on porous organic polymers, supramolecular and smart materials in the field of wearable electronics.

Ruihu Wang

Ruihu Wang received his PhD (2004) from the FJIRSM (Fujian Institute of Research on the Structure of Matter), Chinese Academy of Sciences. Following post-doctoral experience at the University of Idaho and University of Kansas, he became a professor at FJIRSM in 2008. In 2021, he joined Hebei University of Technology and is the director of the School of Chemical Engineering and Technology. His main research interests include porous organic polymers, inorganic–organic hybrid materials for catalysis and energy storage.

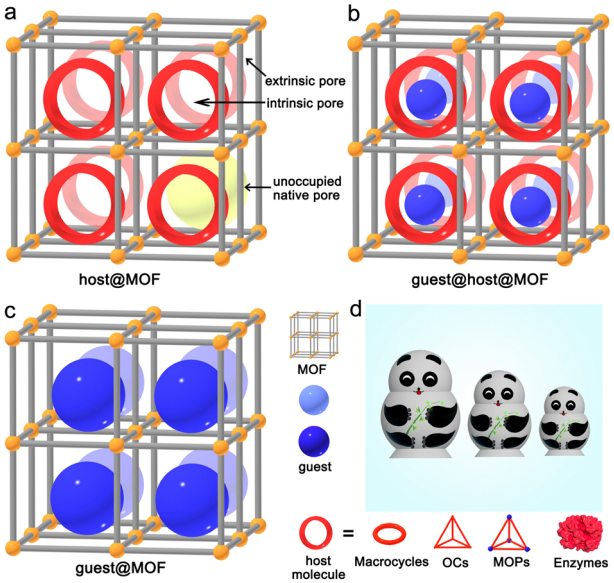

Fig. 1 Schematic views of (a) host@MOF materials composed of MOFs as the host matrix and encapsulated host molecules such as macrocycles, organic cages (OCs), metal–organic polyhedrons (MOPs) or enzymes; (b) guest@host@MOF materials and (c) traditional guest@MOF materials. (d) Russian (Matrjoschka) dolls to symbolize guest@host@MOF materials.

size play a role in mass transfer, accommodation of other guest entities, and a size sieving effect. Importantly, the "host" in the host@MOF can still encapsulate or anchor functional "guest" species to then provide guest@host@MOF materials (Fig. 1b).

For guest@host@MOF materials, one could also differentiate the possibility of guests in the intrinsic pores (Fig. 1b) and guests in the extrinsic pores. Therefore, host@MOF materials should not be mistaken with already widely investigated guest@MOF materials,[26–28] where the "guest" is, however, not capable of further encapsulation of other "guest" molecules (Fig. 1c). The host@MOF calls up the term of Matryoshka dolls, also known as stacking dolls, nesting dolls, or Russian dolls, a set of wooden dolls of decreasing size placed one inside another (Fig. 1d). Compared with simple guest@MOF materials, host@MOF composites have provided new opportunities for the exploration of host–guest chemistry in crystalline matrices like MOFs. Enzymes are included as "host molecules" as many enzymes possess the binding pockets for molecular recognition and subsequent selective catalysis.[7] This review summarizes what has been accomplished to date and what synthetic and characterization tools are available for researchers interested in host@MOF composite materials.

We begin by analyzing the advantages of MOFs as host matrices. Second, we introduce the useful encapsulation approaches and general important considerations. Third, host@MOF materials with various host molecules (Fig. 2, Table S1, ESI†) and enzymes (Table S2, ESI†) are presented. Then, the enhanced performance of these composites for various applications is discussed. Finally, we introduce general characterization methods for host@MOF materials before we address the challenges that need to be overcome to advance host@MOF materials. Hopefully, this review will inspire more interest and enthusiasm in developing new host@MOF and guest@host@MOF materials for various applications.

2. Advantages of metal–organic frameworks as matrices for host molecules

Metal–organic frameworks (MOFs) are potentially porous and largely crystalline materials constructed from organic linkers and metal ions or metal clusters *via* coordination bonds.[29] The pore size, pore volume, and functionalities of MOFs can be tuned by the assembly of judiciously chosen linkers and metal-containing secondary building units (SBUs). The past three decades have seen the rapid development of MOFs and their potential applications including sorption and separation, catalysis, and energy conversion.[30] MOFs have some advantages that make them ideal supports for the encapsulation of various host species, such as macrocycles, organic cages, metal–organic polyhedrons and enzymes. These features are presented in the following points.

(i) Uniform pore structure. MOFs contain uniform micropores up to small mesopores distributed throughout their usually three-dimensionally ordered frameworks. Functional host molecules may be arranged and isolated in the MOF lattice, which should facilitate the interactions between the intrinsic porosity of the host species and other guest molecules. The high porosities of MOFs and their tunable pore size should ensure the access of additional guests to the encapsulated host molecules.

(ii) Tunable pore size. MOFs with various pore sizes can be prepared by varying the length of the organic linker in isoreticular synthesis.[31] In addition to the micro- and small mesopores in defect-free MOFs, hierarchical meso-/macropores can be created by utilizing templating strategies,[32] or using modulators for defective MOFs. The tunable pore size of

Christoph Janiak

Christoph Janiak is full professor for Nanoporous and Nanoscale Materials at the Heinrich Heine University of Düsseldorf since 2010, with research interests in the synthesis and properties of metal and porous organic frameworks (MOFs, COFs), mixed matrix membranes, metal nanoparticles, ionic liquids, and catalysis. He is currently an honorary professor at Wuhan University of Technology and a guest professor at the Hoffmann Institute of Advanced Materials at Shenzhen Polytechnic University in China. He has (co-)authored about 710 research papers and is a Fellow of the Royal Society of Chemistry (FRSC).

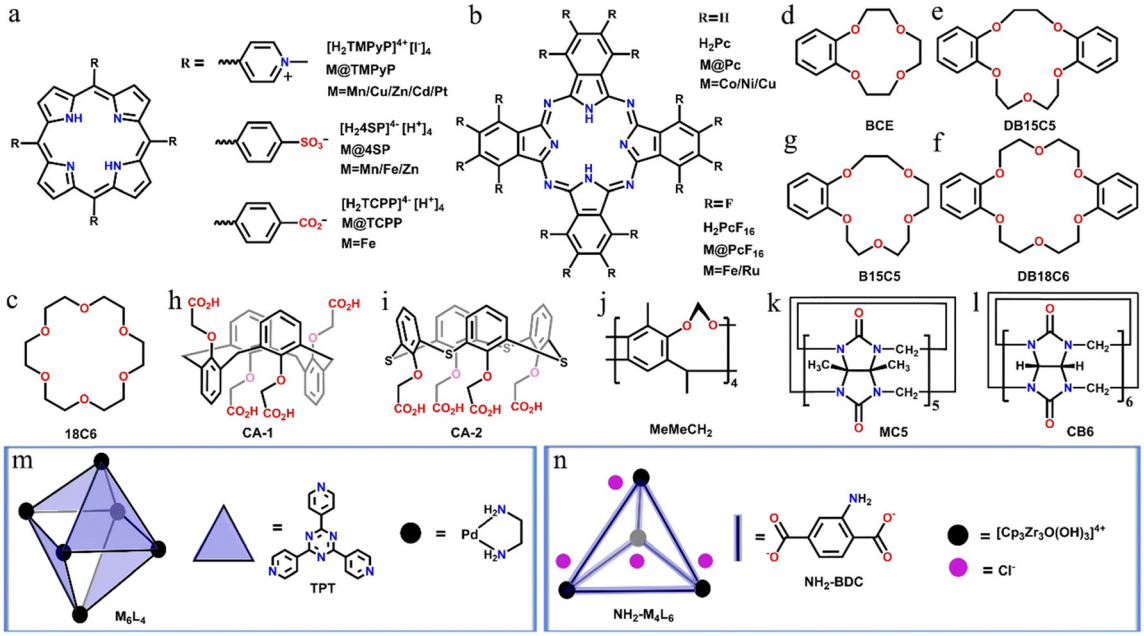

Fig. 2 Representative host molecules to construct host@MOF and guest@host@MOF materials. (a) Cationic and anionic porphyrins (PPs); (b) phthalocyanines (PCs); (c)–(g) crown ethers (CEs); (h) and (i) calixarene derivatives (CAs); (j) Cram's bowl-shaped cavitand; (k) and (l) cucurbiturils (CBs); (m) octahedral and (n) tetrahedral metal–organic polyhedrons (MOPs).

chosen MOFs enables the inclusion of functional host molecules of various sizes and the diffusion of additional guest species (including substrates and products in catalysis) to the host.

(iii) Large pores with small windows. MOFs can contain cage-like pores that are interconnected by small pore windows. For example, MIL-101[33] has two kinds of mesopores with diameters of about 2.9 nm and 3.4 nm, which are only available through pentagonal and hexagonal windows with diameters of about 1.2 nm and 1.5 nm × 1.6 nm, respectively. Thus, MIL-101 could accommodate host molecules in its pores and prevent them from aggregating or leaching.[34] The tunable window size of MOFs may exhibit size sieving effects.

(iv) Tunable pore environment. Pore surface engineering can be implemented in MOFs by pre-/post-synthetic modification of linkers or metal nodes.[35] In this way, MOFs with identical structures but distinctive surfaces can be created to tune the microenvironment and properties of encapsulated host molecules.

(v) Mild synthetic conditions. Great progress has been made in the synthesis of MOFs. Some MOFs (*e.g.* ZIF-8) can be synthesized under very mild conditions.[36] Mild synthetic conditions are important to retain the stability and properties of host molecules during one-pot assembly synthesis.

(vi) Tunable stability. Based on the hard/soft acid–base concept, stable MOFs can be synthesized by the combination of carboxylate linkers and high valence metals (Al^{3+}, Cr^{3+}, Fe^{3+}, Zr^{4+}, Ti^{4+}, *etc.*), or azolate linkers with lower valence metal species (Zn^{2+}, Ni^{2+}, *etc.*).[37] For targeted host@MOF materials, the MOF matrix with proper stability can be designed.

(vii) Shaping. Some strategies for the efficient shaping of MOFs have been developed for exploring their practical applications.[38] It is extremely difficult to prepare porous host molecule-based monolithic materials, while the development of host@MOF materials provides new possibilities.[39]

3. Encapsulation paths and important considerations

Currently, a few approaches have been developed for the successful preparation of host@MOF and guest@host@MOF materials. Generally, these include wetness impregnation synthesis, bottle-around-ship synthesis, and ship-in-bottle synthesis (Fig. 3).

3.1 Wetness impregnation synthesis

Wetness impregnation or infiltration is a widely used method for the preparation of MOF composites, such as ionic liquid@MOF,[40] polyoxometalate@MOF,[41] enzyme@MOF,[42] *etc.* Wetness impregnation synthesis is frequently used to trap host molecules within the pores of MOFs (Fig. 3a). Generally, several factors should be considered: (i) the molecular size of the host molecule should be smaller than the window or channel size of the chosen MOF, in other words, the MOF should have proper inner pore/window pore sizes, to allow the diffusion of the host molecules into the MOF framework. (ii) The host molecule should have good solubilities in a solvent to obtain the impregnation solution with tunable and high enough concentrations. (iii) The MOF should have good chemical and thermal stabilities to tolerate the impregnation conditions. (iv) MOFs might be properly activated before conducting impregnation synthesis. (v) Suitable supramolecular interactions or electrostatic

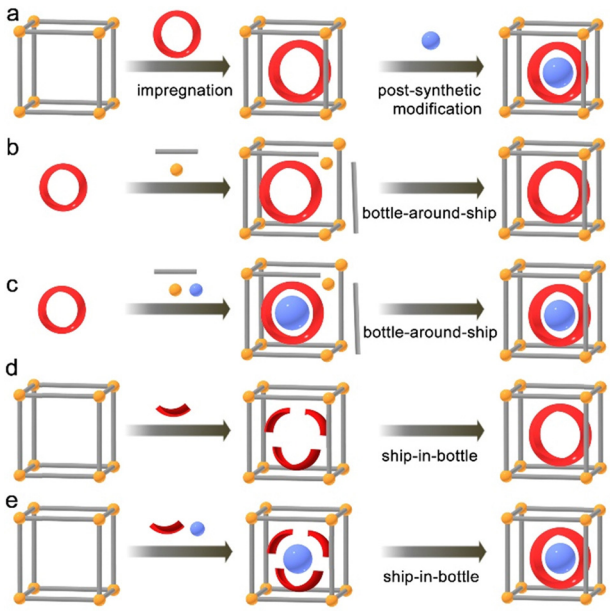

Fig. 3 Synthetic strategies of host@MOF and guest@host@MOF materials. (a) Impregnation synthesis and post-synthetic modification, (b) and (c) bottle-around-ship synthesis, and (d) and (e) ship-in-bottle synthesis. Note: the grey rod represents the organic linker and the gold sphere represents the metal node of the MOF; the blue sphere represents guest species, the red barrel represents host molecules such as macrocycles, organic cages, metal–organic polyhedrons and enzymes, the red fragment represents precursors of host molecules.

adsorption should be helpful for the impregnation process. Successful synthesis of host@MOF can not only achieve a relatively high percentage of host molecules, but also ensures that both MOFs and host molecules remain intact during the infiltration processes.

Impregnation synthesis of host@MOF is simple and fast since MOFs and guest/host species are separately pre-prepared before their mutual integration. The loading amount of host molecules can be well controlled. Post-synthetic modification (PSM) of host@MOF can further lead to guest@host@MOF materials with possible positive structural changes of the host molecule and/or the MOF. It is challenging to ensure the encapsulation of host molecules in all cages of the MOF due to size sieving effects and diffusion limitations, especially when the MOF has small pores and large particle sizes. Thus, the use of nanoscale MOFs for encapsulation through this approach is advantageous. Depending on the encapsulation degree and position of the host molecule in the MOF, the host@MOF material should possess intrinsic pores/cavities, extrinsic pores, and possible native pores of the MOF. There exists a trade-off between the host molecule loading amount and the native pores of the MOF. Impregnation synthesis is suitable for soluble or sensitive host molecules such as enzymes.

3.2 Bottle-around-ship synthesis

When a host molecule has a larger kinetic molecular size than the window pore size of MOFs, wetness impregnation would be difficult. Bottle-around-ship synthesis can circumvent this problem by mixing host molecules with ligands, and metal ions under the required MOF synthesis conditions to obtain the host@MOF materials (Fig. 3b). Bottle-around-ship synthesis can be applied when the following factors are met. (i) The kinetic molecular size of the host molecule is smaller than the inner pores of the MOF. For some large enzymes, the preparation of enzyme@MOF materials can be achieved by ''coprecipitation'' or ''biomineralization'', which encapsulate enzymes in the superstructures of MOFs and therefore are not limited by the pore size of MOFs.[42] (ii) Host molecules have good solubility and stability in the solvent and mixtures where MOFs can be readily formed. (iii) Host molecules cannot form strong interactions with the MOF precursors (*e.g.* metal ions or ligands). Rather, weak to moderate interactions may be formed between host molecules and the MOF precursors, but the intrinsic properties of the host molecules remain intact in the host@MOF materials. In some cases, metal ions can be anchored on host molecules to form metal@host@MOF materials *via in situ* (Fig. 3c), pre-synthetic or post-synthetic modifications (Fig. 3a) (Section 4.1). (iv) The synthesis conditions of MOFs should be relatively mild to keep the structure of host molecules intact in the material.

Bottle-around-ship synthesis has been successfully applied for the synthesis of some host@MOF materials. This strategy has the potential to entrap host molecules in all cages of the MOF due to a size matching effect and the assembly at the molecular level, especially when the MOF has a single type of cage such as ZIF-8. Single crystals might be obtained *via* this approach to analyse the detailed structures of the host@MOF including the position and microenvironment of the host and porosities, *etc.* Depending on the position of the host molecule in the MOF, the host@MOF material can possess intrinsic pores, extrinsic pores, and possible native pores of the MOF. Certainly, clear structures should be helpful for the study of structure–function relationships. It is noted that some host molecules can be used as templates for the direction and stabilization of the obtained MOF that otherwise cannot be prepared. This strategy is suitable for soluble and relatively stable host molecules including porphyrins, crown ethers, MOPs, and enzymes.

3.3 Ship-in-bottle synthesis

Ship-in-bottle synthesis means that host molecules as the 'ship' are *in situ* formed in the pores of the MOF as the 'bottle',[34] which requires first the impregnation of ions and/or molecular precursors into the pores of MOFs (Fig. 3d). This method can avoid a series of troublesome issues including low solubility of host molecules, and larger molecular size than the pore window size of the MOF. Ship-in-bottle synthesis can be used when the following factors are met. (i) The precursors of the host molecule can be impregnated into the pores of the MOF, and the host molecule can be easily synthesized or assembled based on covalent bonds or coordination bonds under relatively mild conditions. (ii) The kinetic molecular size of the host molecule should be smaller than the intrinsic micro-/meso-pores of the

MOF. (iii) The stability of the MOF should tolerate the synthetic conditions of the host molecules.

Ship-in-bottle synthesis has also been applied for the synthesis of a few host@MOF materials. This strategy relies on the use of stable MOFs containing mesopores that provide enough space to permit the confined assembly of host molecules. Depending on the amount and position of the host molecule in the MOF, the host@MOF material should possess intrinsic pores, extrinsic pores, and possible native pores of the MOF. Moreover, guest@host@MOF materials might be *in situ* formed during the bottle-around-ship synthesis (Fig. 3e) or *via* PSM (Fig. 3a). It is challenging to confirm the intact structure and position of the host molecules. This strategy is suitable for host molecules that can be easily assembled in the mesopores of stable MOFs.

Based on the synthetic approaches sketched in sections 3.1 to 3.3, some representative host@MOF, related guest@host@MOF and enzyme@MOF materials are reported and summarized in Tables S1 and S2 (ESI†).

4. Functional host@MOF and guest@host@MOF materials

Up to now, only a few kinds of macrocycles, polyhedrons and enzymes have been encapsulated into the pores of MOFs to obtain composites and bio-composites materials with enhanced properties. Herein, we have comprehensively reviewed the syntheses and structures of host@MOF and guest@host@MOF materials based on the types of host molecules (Scheme 1).

4.1 Porphyrin@MOF materials

Porphyrins are a class of heterocyclic molecules containing four pyrrole subunits linked by methylene bridges. In nature, porphyrins occur in coordination with metal ions. Metal porphyrins (M@PP) and their derivatives are widely found in organelles related to energy transfer and play indispensable roles in various metabolic processes such as light-harvesting (*e.g.* chlorophyl II), O_2 transport and activation (*e.g.* hemoglobin and hemocyanin), and many catalytic reactions. This has inspired researchers to synthesize many metal-coordinated porphyrin molecules and construct biomimetic systems, including the integration of metalloporphyrins in crystalline porous frameworks.[43] Encapsulation approaches are taken to obtain M@PP@MOF materials with a controlled microenvironment of metalloporphyrin active sites.

Alkordi *et al.*[44] successfully achieved the encapsulation of the cation of $[H_2TMPyP]^{4+}[p\text{-tosyl}^-]_4$ (*cf.* Fig. 2a) into the cages (diameter of the window size: 9 Å) of an anionic MOF (MOM-2) to obtain H_2TMPyP@MOM-2 *via* a bottle-around-ship synthesis (Fig. 4). Interestingly, post-synthetic metalation of the encapsulated free-base porphyrin was conducted by immersing the composite in various solutions of transition metal ions to give M@TMPyP@MOM-2 (M = Mn^{2+}, Cu^{2+}, Zn^{2+}, Co^{2+}). Later, Masih *et al.*[45] encapsulated Pt@TMPyP into the same In^{3+}-based MOM-2 to fabricate Pt@TMPyP@MOM-2 for anion-selective photoluminescence (PL) sensing. They found that negligible PL changes were observed for iodide ions, while obvious PL "turn off" occurred with sulfide ions, which caused the decomposition of the MOF and release of Pt@TMPyP, resulting in its availability for the photoinduced electron transfer reaction.

Larsen *et al.*[46] reported a class of MOFs that mimic heme enzymes (termed MOMzymes). Notably, catalytically active metalloporphyrins are selectively encapsulated within the octahedral cages of the prototypical HKUST-1(Cu, Zn) framework in a "bottle-around-ship" fashion, thus creating functional and orientationally specific proximal and distal heme pockets as well as substrate selective access channels to and from the porphyrin active sites (Fig. 5). The designated M@4SP@HKUST-1 (M = Fe(III), Mn(III), 4SP = tetrakis(4-sulphonatophenyl)porphyrin, *cf.* Fig. 2a, middle) materials have a tunable amount of the porphyrin. The good peroxidase activity of Fe@4SP@HKUST-1(Cu) is demonstrated in the degradation of H_2O_2 due to the well accessible active Fe@4SP units within the octahemioctahedral cages of the framework.

Porphyrins can be used as a template for the synthesis of new MOFs. Zhang *et al.*[47] reported a series of M@TMPyP@MOM-*n* (*n* = 4, 5, 6) by utilizing the porphyrin salt ($[H_2TMPyP]^{4+}[I^-]_4$) as a template, whereby *in situ* formed metalloporphyrins were selectively trapped within the cages of resultant MOFs. M@TMPyP@MOM-*n* (M = Fe^{2+}, Co^{2+}, Mn^{2+}, respectively) are isostructural with HKUST-1 with the twisted boracite (tbo) topology (Fig. 5). There are three types of polyhedron cages with 1 : 1 : 2 stoichiometry: rhombihexahedral, octahemioctahedral, and octahedral in the framework. Like in M@4SP@HKUST-1(Cu), M@TMPyP can only be encapsulated

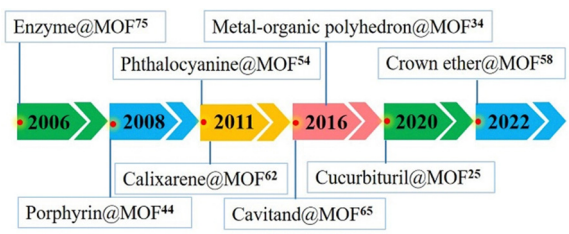

Scheme 1 Timeline of the milestones of host@MOF and guest@host@MOF materials.

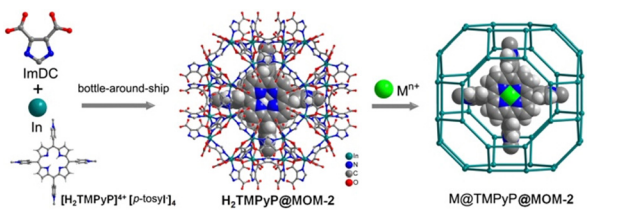

Fig. 4 View of the bottle-around-ship synthesis of H_2TMPyP@MOM-2 *via* the encapsulation of H_2TMPyP porphyrin cation in the anionic MOF named MOM-2, and the synthesis of M@TMPyP@MOM-2 *via* post-synthetic metalation. Adapted from ref. 44 with permission of the American Chemical Society, Copyright 2008.

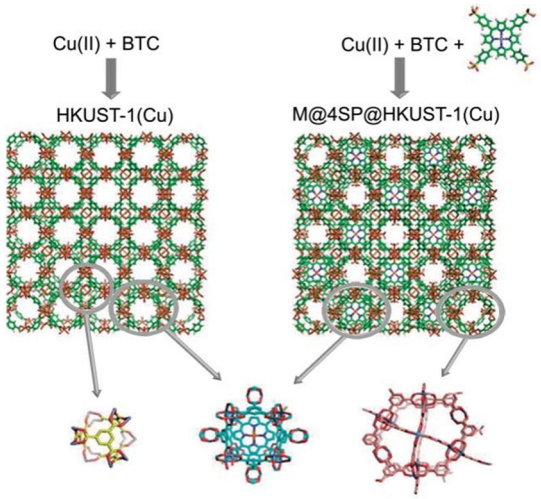

Fig. 5 The encapsulation of the metalloporphyrin M@4SP within the cages of HKUST-1(Cu) to form M@4SP@HKUST-1(Cu) *via* a bottle-around-ship synthesis. The other cavities associated with the framework are also illustrated. Reproduced from ref. 46 with permission of the American Chemical Society, Copyright 2011.

in the octahemioctahedral cage while the other two kinds of cages are empty and allow for substrate diffusion.

Zhang *et al.*[48] reported another anionic Cd-based MOM that contains *in situ* formed Cd@TMPyP (*cf.* Fig. 2a), which was termed as Cd@TMPyP@MOM-10(Cd). There is a 1 : 1 ratio of two types of square channels: (A) 12.6 Å × 12.6 Å; (B) 11.9 Å × 11.9 Å. Cd@TMPyP stacked in channels A, separated by 10.3 Å, and was trapped in cuboid boxes. Interestingly, the composite can be transformed to Mn@TMPyP@MOM-10(Mn) for catalysis *via* single-crystal to single-crystal transformation. Zhang *et al.*[49] also reported the Cd@TMPyP@MOM-11(Cd) that consists of an anionic framework with encapsulated cationic Cd@TMPyP (*cf.* Fig. 2a, top) in alternating channels. Cd@TMPyP@MOM-11(Cd) exhibited approximately 11.0 Å × 11.0 Å square channels, and half of the channels were occupied by Cd@TMPyP moieties. The weakly bonded axial oxygen atom on Cd of the Cd@TMPyP moiety is amenable to replacement by anionic ligands (Fig. S1, ESI†). Interestingly, Cd@TMPyP@MOM-11(Cd) enabled stoichiometric addition of metal chloride salts (*e.g.* NaCl, $BaCl_2$, $CdCl_2$, $MnCl_2$) with coordination of metal ions to the walls of the MOM and binding of Cl^- ions to the metalloporphyrin moieties.

Inspired by these works, He *et al.*[50] encapsulated $[Mn@TMPyP]^{4+}[I^-]_4$ into the neutral framework of ZIF-8 *via* a "bottle-around-ship" fashion to obtain Mn@TMPyP@ZIF-8. Sharma *et al.*[51] immobilized $[Zn@TMPyP]^{4+}[I^-]_4$ in the channels of PCN-224 *via* the impregnation method to obtain Zn@TMPyP@PCN-224. Ling *et al.*[52] achieved the encapsulation of functional Fe@TCPP (*cf.* Fig. 2a, bottom) in HKUST-1(Cu) *via* a bottle-around-ship synthesis under mild conditions and demonstrated it to be a good electrochemical indicator for signal readout in electrochemical DNA sensing.

For porphyrin@MOF materials, the charge, chemical stability, channel or cage shape and size of the MOF are very important to accommodate metalloporphyrin molecules for potential applications. Most of the reported porphyrin@MOF materials had very limited chemical stabilities and micropores, which limited their practical applications. Stable and mesoporous MOFs might be employed for more biomimetic materials in the future.

4.2 Phthalocyanine@MOF materials

Metal phthalocyanine (M@Pc) complexes have various applications including catalysis (*cf.* Fig. 2b, top).[53] Unfortunately, M@Pcs usually self-assemble to oligomeric structures in solution through π–π stacking, which strongly limits their catalytic applications in homogeneous systems. Encapsulation of M@Pc into a MOF provides a path to overcome this issue.

Kockrick *et al.*[54] used impregnation synthesis to encapsulate a series of M@Pc complexes in the mesopores (diameter 2.9 nm and 3.4 nm) of MIL-101 for the selective oxidation of tetralin into 1-tetralone. The catalytically active two different perfluorinated M@Pc complexes ($M@PcF_{16}$, M = Fe, Ru) (*cf.* Fig. 2b, bottom) were incorporated into the porous structure due to their smaller size (1.3 nm × 1.3 nm) than the hexagonal pore windows (1.5 nm × 1.6 nm) of MIL-101. In contrast, the bulky dimer $(FePc^tBu_4)_2N$ was only adsorbed at the outer surfaces of MIL-101 crystallites due to its large size (~2.0 × 2.0 nm).

While wetness impregnation is limited by the solubility of Pc molecules, and by the window pore size of the MOF, "ship-in-bottle" synthesis can circumvent these issues. Li *et al.*[55] developed a metal-cation-directed *de novo* assembly strategy to encapsulate various M@Pc's (molecular dimensions ~1.3 nm × 1.3 nm) in the pores of bio-MOF-1 (window size ~1.0 nm × 1.0 nm) (*cf.* Fig. 2b, top and Fig. 6). The authors chose an anionic framework as bio-MOF-1 with 1D channels in which $Me_2NH_2^+$ cations reside as counterions. After the $Me_2NH_2^+$ cations were exchanged with Co^{2+} ions, Co@bio-MOF-1 was achieved. Then Co@bio-MOF-1 was placed in a solution of 1,2-dicyanobenzene before solvothermal treatment to trigger the *in situ* formation of cobalt(II) phthalocyanine (Co@Pc) in bio-MOF-1. Various M@Pc@bio-MOF-1 (M = Co^{2+}, Ni^{2+}, Cu^{2+}) materials were obtained.

Later, Boroujeni *et al.*[56] used the "ship-in-bottle" synthesis strategy to obtain M@Pc@MIL-101. Metal ions are first doped into the pores of MIL-101(Cr) *via* the double solvent method. Then M@MIL-101 was suspended in an ethanol solution of 1,2-dicyanobenzene before thermal treatment in an ionic liquid to afford M@Pc@MIL-101 (M = Cu^{2+}, Co^{2+}, Ni^{2+}). Cu@Pc@MIL-101

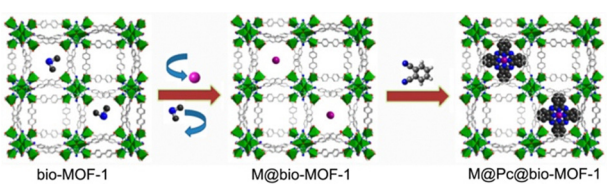

Fig. 6 Schematic presentation of ship-in-bottle synthesis of M@Pc@bio-MOF-1 (M = Co^{2+}, Ni^{2+}, Cu^{2+}). Reprinted from ref. 55 with permission of the American Chemical Society, Copyright 2014.

shows high stability and excellent catalytic performance in the oxidative amidation of aldehydes with amine salts. Yegneh *et al.*[57] used the same strategy but a deep eutectic solvent (DES) and a lower temperature to obtain Cu@Pc@MIL101(Cr) and Cu@Pc@MIL100(Fe) as catalysts for the catalytic epoxidation of styrene with molecular oxygen as an oxidant.

Compared with PP@MOF, Pc@MOF materials were relatively less studied, and ship-in-bottle synthesis was generally used. As Pc's have unique photo-/electro-chemical properties, new synthetic paths may be taken to construct more Pc@MOF materials for photo-/electrocatalysis.

4.3 Crown ether@MOF materials

Crown ethers (CEs) represent the second generation of macrocyclic host molecules. Crown ethers are defined as the macrocyclic oligomers of ethylene oxide in the form of $(-CH_2CH_2O-)_n$ with $n \geq 4$.[12] The oxygen atoms in crown ethers are well situated to form coordination or electron donor–acceptor interactions with guests (*e.g.* metal cations and organic cations) located in the interior of the macrocyclic polyethers, while the exterior of the macrocycles is hydrophobic which endows the complexed cation with good solubility in organic solvents. CEs have been widely studied and found applications in various fields including catalysis, recognition and separation, analysis, molecular drug design and smart materials. Recently, crown ethers have been encapsulated in MOFs to fabricate CE@MOF materials with enhanced ion transport performances.[58–61]

Ma *et al.*[58] first proposed the strategy of encapsulating a crown ether into the subnanochannels of MOFs for improving the alkali metal ion selectivity. They successfully fabricated devices that contain 18C6@ZIF-67/18C6@ZIF-8 prepared on asymmetrically structured silicon nitride (SiNx) by atomically thin nanoporous graphene (NG)-assisted *in situ* step-by-step liquid phase construction. Notably, the device showed enhanced Li^+ conductivity and enhanced selectivity for Li^+/K^+ and Na^+/K^+, respectively, than those of the plain ZIF-67/ZIF-8/NG.

Li *et al.*[59] encapsulated benzo-12-crown-4-ether (BCE) (*cf.* Fig. 2d) in the anionic ZIF-7 to obtain a BCE@ZIF-7 membrane *via* a bottle-around-ship synthesis (Fig. 7a). BCE can be well trapped in the micropores of ZIF-7 due to its smaller size (8 Å) than the cavity size (~8.7 Å), but larger than the pore window size (4.9 Å) of ZIF-7. BCE@ZIF-7 was further converted to M@BCE@ZIF-7 (M = Li^+, Mg^{2+}, Al^{3+}) after binding various metal cations to BCE. The channel charges of M@BCE@ZIF-7 changed from negative to positive based on zeta potential analysis results, whereby ZIF-7 and Li@BCE@ZIF-7 exhibited electrostatic attraction with Li^+ and Mg^{2+} ions while M@BCE@ZIF-7 (M = Mg^{2+}, Al^{3+}) resulted in electrostatic repulsion instead. Remarkably, the positively charged membrane (Al^{3+}@BCE@ZIF-7) achieved the highest Li^+/Mg^{2+} selectivity of *ca.* 125 (Fig. 7b).

Xu *et al.*[60] used a robust Zr-MOF to confine various CEs in the microporous cages of UiO-66. They successfully loaded dibenzo-15-crown-5 (DB15C5) or dibenzo-18-crown-6 (DB18C6) (*cf.* Fig. 2e and f) into the *in-situ* formed UiO-66 on the anodic alumina oxide (AAO) substrates to obtain a CE@UiO-66

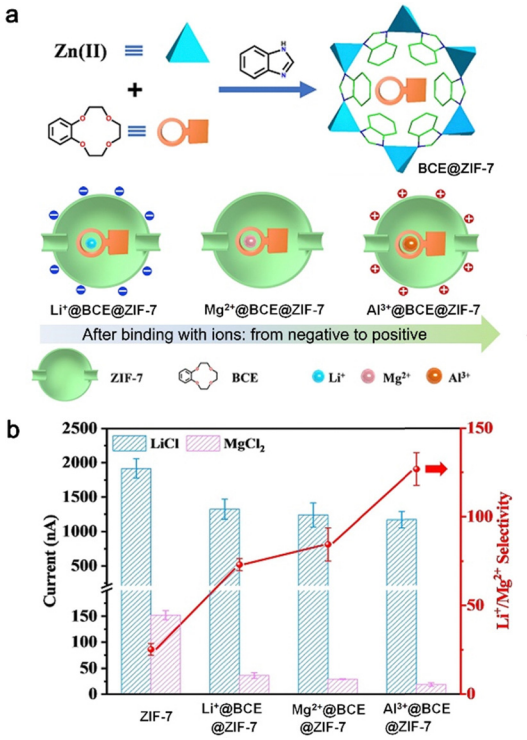

Fig. 7 Preparation of M@BCE@ZIF-7 (M = Li^+, Mg^{2+}, Al^{3+}) with a change of channel charges from negative to positive. (b) Current values across various membranes and the corresponding Li^+/Mg^{2+} selectivity. Reproduced from ref. 59 with permission of Wiley-VCH Verlag GmbH & Co, Copyright 2023.

membrane called DB15C5@UiO-66 and DB18C6@UiO-66 (Fig. 8a). UiO-66 possesses tetrahedral cages of ~6 Å and octahedral cages of ~12 to 15 Å diameter, the latter can perfectly accommodate DB18C6 and DB15C5 with molecular sizes around 12 Å and hinder the leaching of CE due to the smaller window aperture of 8 Å (Fig. 8b). Notably, compared with a UiO-66 membrane on the AAO substrate, CE@UiO-66 membranes exhibit greatly enhanced selective mono-/divalent

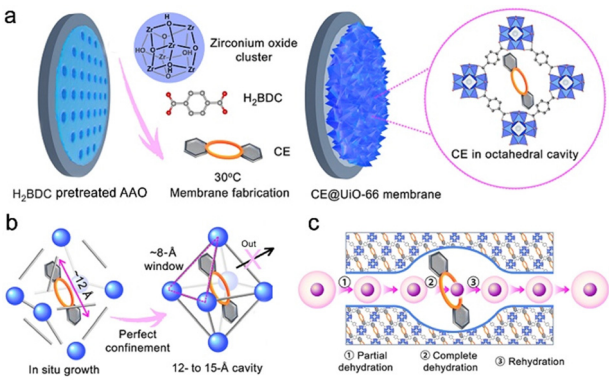

Fig. 8 (a) Fabrication of CE@UiO-66 membranes, such as DB15C5@UiO-66 and DB18C6@UiO-66. (b) Perfect confinement of CE (~12 Å) in the UiO-66 cage. (c) Size and interaction sieving of monovalent ions in CE@UiO-66 membranes. Adapted from ref. 60 with permission of the American Association for the Advancement of Science, Copyright 2024.

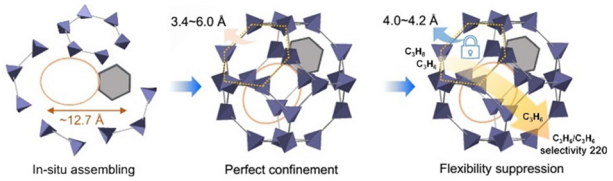

Fig. 9 Schematic view of perfect confinement of B15C5 within ZIF-8 nanocages for the suppression of framework flexibility, thus enhancing C_3H_6/C_3H_8 separation. Adapted from ref. 61 with permission of Wiley-VCH Verlag GmbH & Co, Copyright 2024.

ion transport due to combination of the precise pore size sieving effect and interaction screening effect as well as the complete dehydration of monovalent ions (Fig. 8c).

Zhang *et al.*[61] embedded a crown ether within a ZIF-8 membrane to fine-tune the flexible pore structure of ZIF-8. Benzo-15-crown-5 (B15C5) (*cf.* Fig. 2g) was perfectly entrapped in the cage of ZIF-8 *via* bottle-around-ship synthesis. Theoretical simulations suggested the comparable size of B15C5 to the nanocage (diameter 12 Å) of ZIF-8, which imposes a spatial constraint on linker rotation thus transforming the flexible ZIF-8 phase to a rigid structure for enhanced C_3H_6/C_3H_8 separation (Fig. 9).

CE@MOF materials have become a fast-growing subclass of host@MOFs and show promising results in energy and separation fields. Due to the large number of CEs and MOFs, it is expected that more CE@MOF materials can be fabricated for various applications in the future.

4.4 Calixarene@MOF materials

Calixarenes represent the third generation of macrocyclic host molecules after CDs and crown ethers. Calixarenes (CAs) can be prepared easily by the condensation of commercially available phenols and formaldehyde.[12] CAs are composed of phenolic units linked by methylene bridges or heteroatoms at their *meta*-positions and usually possess a cup-like shape with two rims. The hydrophobic cavities of CAs can capture smaller molecules and ions through hydrophobic and various supramolecular interactions. Thus, the host–guest/supramolecular chemistry of CAs and derivatives has been widely investigated in both solution and the solid state.

Isaeva *et al.* incorporated two functional calix[4]arene molecules (CA-1 and CA-2) (*cf.* Fig. 2h and i) with carboxylic acid groups into MOF-5(Zn) *via* a ''bottle-around-ship'' synthesis to form CA-1@MOF-5 and CA-2@MOF-5 materials.[62] The incorporation of CA in the MOF led to a higher fraction of the amorphous phase and interlacing lattice structures as the content of calixarene grew. Later, Isaeva *et al.* used the calix[4]arene@MOF-5 materials as supports to anchor the Pd catalyst for stereoselective hydrogenation of 2-butyne-1,4-diol into *cis*-2-butene-1,4-diol. In catalysis studies, Pd@calix[4]arene@MOF-5 with carboxylate groups on the calix[4]arene (Fig. 2i) led to enhanced activity as compared with Pd@MOF-5 and Pd/C.[63]

Although the CA@MOF concept was reported since 2011, the development of CA@MOF materials is sluggish compared with CA-based MOFs.

4.5 Cavitand@MOF materials

Many simple cavitands can show gas sorption capabilities, but most of them exhibit low permeabilities. Encapsulation of cavitands in the pores of ZIFs stands for a useful approach to explore their properties with the advantages that:[64] (i) they have recognition sites in the pores, (ii) they may act as structure-directing agents for larger-pore ZIFs, and (iii) they may, by virtue of their rigidity, stabilize the frameworks of large pore ZIFs.

Ramirez *et al.*[65] used Cram's bowl-shaped cavitand, MeMeCH$_2$ (*cf.* Fig. 2j), as a template to direct the synthesis of ZIF-10 ($Zn_{16}(Im)_{32}$) that is otherwise difficult to synthesize (Fig. 10). In the ''bottle-around-ship'' synthesis of MeMeCH$_2$@*mer*-ZIF-10 (Fig. 10b and c), MeMeCH$_2$ played a key role in templating the double-eight ring (*d8r*) of the *mer*-ZIF-10. Notably, one MeMeCH$_2$ molecule resided in each of the *d8r*. This was supported by the C–H$\cdots$O hydrogen bonds (C$\cdots$O = 3.135 Å) between imidazolate ''struts'' of *d8r* and MeMeCH$_2$ template (Fig. 10d). The authors were unable to prepare *mer*-ZIF-10 free of cavitand and only obtained ZIF-4. MeMeCH$_2$@*mer*-ZIF-10 has a highly porous and thermally stable structure up to 80 °C, and a BET surface area of 1893 $m^2\ g^{-1}$.

Brekalo *et al.*[64] also discovered another phase of $ZnIm_2$, namely MeMeCH$_2$@*rho*-$Zn_{16}(Im)_{32}$ by bottle-around-ship synthesis. In the material (Fig. 11), MeMeCH$_2$ functions as an effective template for the double-eight-ring (*d8r*) motif almost identical to the previously reported MeMeCH$_2$@*mer*-ZIF-10 (Fig. 11b and c). But unlike the *mer* material, only half of the *d8r* rings in the *rho* material are filled with the cavitand for steric reasons. Finally, they were able to obtain the *rho* material as a pure phase from ZnO : HIm : MeMeCH$_2$: DEF = 1 : 2 : 0.5 : 4 *via* mechanochemical synthesis under liquid-assisted grinding conditions. It is noteworthy that MeMeCH$_2$ played a pivotal template role in the formation of this *rho* material (Fig. 11d), which otherwise, cannot be obtained without MeMeCH$_2$. Although these two cavitand@ZIF materials are among the rare

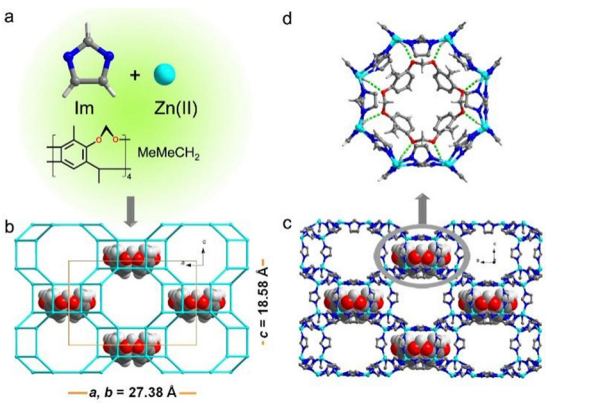

Fig. 10 The synthesis and structural features of MeMeCH$_2$@*mer*-ZIF-10. (a) Imidazolate, zinc ion, and MeMeCH$_2$ as precursors of materials. (b) Wireframe and (c) ball-and-stick view of the *mer*-ZIF-10 framework, occupied by cavitands. (d) Top view of MeMeCH$_2$ situated in the double-eight ring of *mer*-ZIF-10. Adapted from ref. 65 with permission of the American Chemical Society, Copyright 2014.

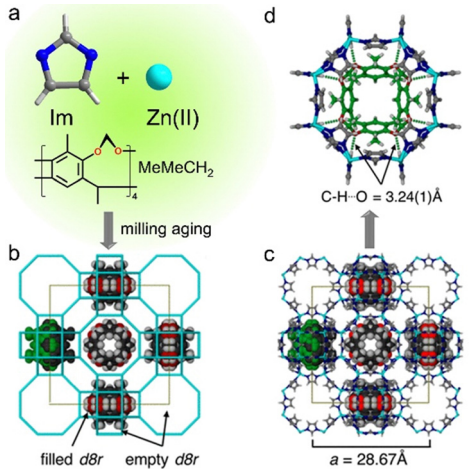

Fig. 11 The mechanochemical synthesis and structural features of MeMeCH$_2$@*rho*-Zn$_{16}$(Im)$_{32}$. (a) Imidazole, zinc salt, and MeMeCH$_2$ as precursors of materials. (b) Wireframe and (c) ball-and-stick representation of the *rho*-ZnIm$_2$ framework, occupied by MeMeCH$_2$. (d) Top view of the MeMeCH$_2$@*d8r* motif. Adapted from ref. 64 with permission of the American Chemical Society, Copyright 2018.

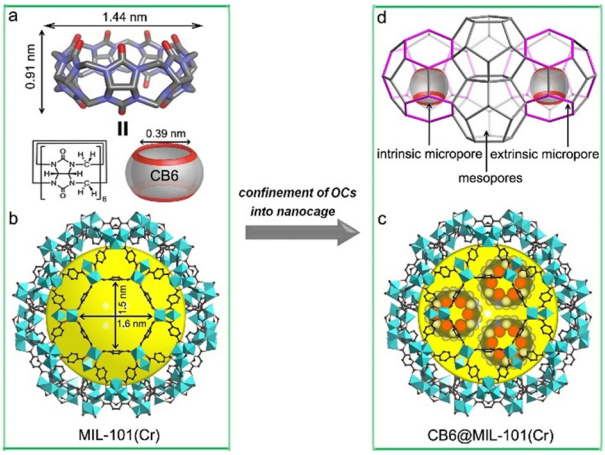

Fig. 12 Illustration of the impregnation synthesis of CB6@MIL-101 materials. Views of (a) CB6 molecule; (b) mesoporous cage with hexagonal windows in MIL-101; (c) CB6s in the larger cage of MIL-101; (d) CB6 being selectively doped into the larger cages in MIL-101 while leaving the smaller cages empty. Adapted from ref. 25 with permission of Wiley-VCH Verlag GmbH & Co., Copyright 2020.

examples of host@MOF materials characterized by single crystal X-ray diffraction, their potential functions, and structure–property relationship remain to be explored.

4.6 Cucurbituril@MOF materials

Cucurbit[*n*]urils (CBn, n = 5, 6, 7, 8, 10)[66] represent a class of highly symmetric macrocycles or simple organic cages with two windows of the same size, which have found applications in host–guest recognition, sorption, catalysis, and smart materials, *etc.*[67] CBs can be easily synthesized by the condensation of formaldehyde and glycolurils. Up to now, CB-based supramolecular frameworks[68] and many coordination polymers[69] have been reported. Nevertheless, it is challenging to prepare CB-based porous solids due to their relatively inert structure, strong tendency to aggregate, and relatively inert structure of CBs. Alternatively, CBn can be confined in the pores of MOFs to afford CB@MOF materials.

Liang *et al.*[25] have encapsulated CB6 cages (*cf.* Fig. 2l) into a stable mesoporous MOF *via* an impregnation method at room temperature (Fig. 12). The key to the synthesis lies in the match between the CB6 size (kinetic diameter 1.44 nm) and the hexagonal window size (1.5 nm × 1.6 nm) of MIL-101 (pore diameter 3.40 nm), the good solubility of CB6 and the excellent acid stability of MIL-101(Cr) in hydrochloric acid. However, CB6 could not enter the smaller mesopore (2.90 nm). Since CB6 has a hydrophobic cavity with a diameter of 5.8 Å and two symmetric hydrophilic windows with a diameter of 3.9 Å, the obtained composites exhibit hierarchical pores with intrinsic pore, extrinsic pore and unoccupied native pores (Fig. 12d). The encapsulated CB6 amount can be controlled by tuning the concentration of CB6 solutions to obtain CB6@MIL-101-*W* (W = 19, 29 or 36 weight% of CB6). The CB6@MIL-101 materials demonstrated an enhanced gas sorption and a better CO$_2$/N$_2$ and CO$_2$/CH$_4$ separation performance than MIL-101 due to the high CO$_2$ affinity of encapsulated CB6. Later, Sun *et al.*[70] found that the impregnation synthesis in hydrochloric acid solutions had actually yielded a CB6@MIL-101-Cl material where the OH$^-$ ligand on the {Cr$_3$(O)(OH)(H$_2$O)$_2$} node of MIL-101 had been partly exchanged with Cl.

Liang *et al.*[39] developed another approach to first prepare a "flowing gel" containing decamethylcucurbit[5]uril (MC5) cages (*cf.* Fig. 2k), the iron salt and BTC linkers of the MOF precursors. Then, the gel was heated to prepare CB@MOF materials *via* the "bottle-around-ship" synthesis (Fig. 13). The chosen cage molecule MC5 has an outer diameter of 1.50 nm,

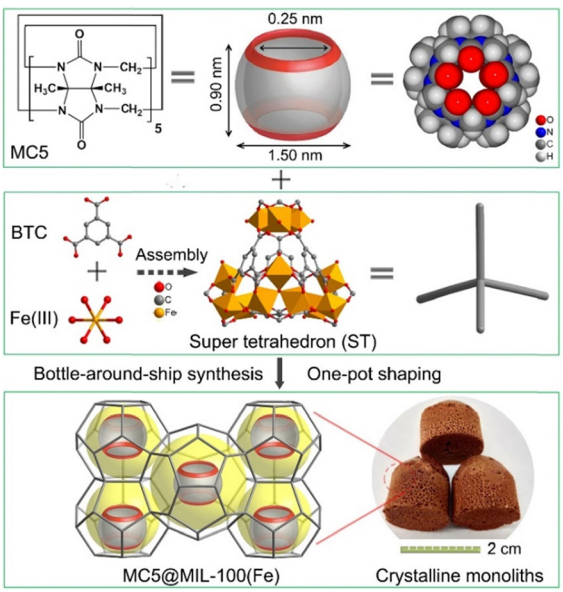

Fig. 13 Schematic view of the "bottle-around-ship" synthesis of monolithic MC5@MIL-100(Fe). Adapted from ref. 39 with permission of Wiley-VCH Verlag GmbH & Co., Copyright 2021.

which is smaller than the two kinds of mesoporous cages (2.50 nm, 2.90 nm). Moreover, the very small MC5 apertures (2.5 Å) would remain accessible in the fabricated composites. The simple grinding and heating operation afforded monolithic MC5@MIL-100(Fe) materials with hierarchical micro-, meso- and macropores.

It would be very helpful to develop a general synthetic method for the construction of CB@MOF materials for the exploration of CB6-based host–guest chemistry in various fields.

4.7 Metal organic polyhedron@MOF materials

Metal–organic polyhedra (MOPs) are a class of inorganic–organic discrete coordination cages, which are prepared by the assembly of metal ions and directional ligands.[71] MOPs have various applications from sensing to catalysis, but their applications are limited due to their low accessible surface areas in the solid state. The encapsulation of MOPs into the pores of MOFs can circumvent these problems by combining the properties of MOPs with the high surface areas and stabilities of MOFs.[34]

Qiu *et al.*[34] successfully encapsulated a MOP in the pores of a stable MOF *via* "ship-in-bottle" synthesis (Fig. 14). A hollow octahedral M_6L_4 cage with a size of about 2.20 nm was chosen for its catalysis capability, in which M represents (en) Pd^{2+} (with two NO_3^- counterions; en = ethylenediamine) and L represents for 1,3,5-tris(4-pyridyl)-2,4,6-triazine (tpt) (Fig. 14a, *cf.* Fig. 2m). Interestingly, the authors developed a hydrophilicity-directed approach to encapsulate the M_6L_4 cages in the mesopores (2.90 nm and 3.40 nm) of MIL-101(Cr) (Fig. 14b). Typically, activated MIL-101(Cr) and soluble L were first mixed in *n*-hexane, and then, a small amount of aqueous M solution ($V_{solution} < V_{pore}$ of MOF) was readily incorporated into the pores in this two-solvent system. Moreover, L was drawn into the MIL-101 pores due to the easy assembly of M_6L_4 in water. As a result, M_6L_4@MIL-101(Cr) was prepared by tuning the concentration of precursors under the reaction conditions.

Similarly, an NH_2-MOP (*cf.* Fig. 2n) was encapsulated in the pores of the Zr-MOF DUT-68 *via* "ship-in-bottle" synthesis,

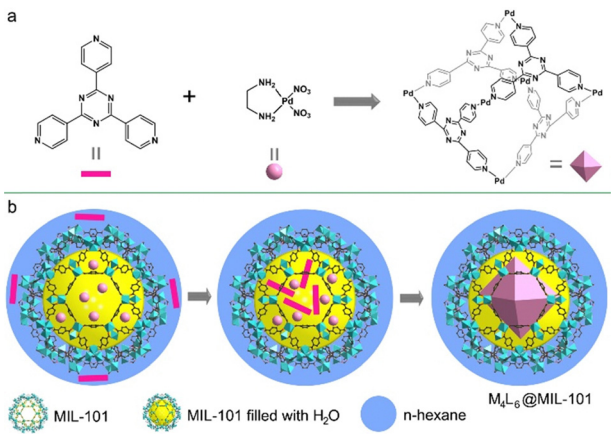

Fig. 14 (a) Schematic preparation of M_6L_4 cages, and (b) the "ship-in-bottle" synthesis of M_6L_4@MIL-101(Cr). Reproduced from ref. 34 with permission of the American Chemical Society, Copyright 2016.

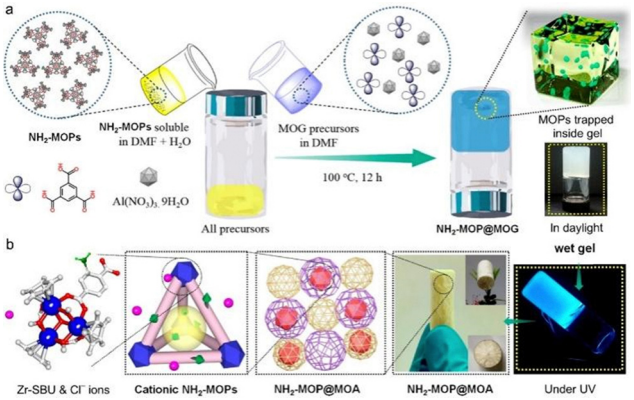

Fig. 15 (a) Schematic preparation of the cationic NH_2-MOP@MOG composite material *via* the "bottle-around-ship" synthesis; the wet-gel composite in daylight. (b) From left to right: Illustration of the Zr-SBU; surrounding free Cl^- ions of NH_2-MOP; NH_2-MOP@MOA; the lightweight composite aerogel form of NH_2-MOP@MOA; the wet-gel composite is luminescent. Adapted from ref. 74 with permission of Wiley-VCH Verlag GmbH & Co., Copyright 2022.

where the NH_2-MOP precursors including BDC-NH_2 ligands and Cp_2ZrCl_2 were impregnated into the DUT-68, and then the NH_2-MOP were assembled in the cage to obtain NH_2-MOP@DUT-68 (Fig. S2, ESI†).[72] DUT-68 contains a large rhombicuboctahedron cage with a diameter of about 2.8 nm and square windows of 1.4 nm, which allows the imbedding of NH_2-MOP and prohibits the leaking. The wetness impregnation approach has also been employed to incorporate nanosized cuboctahedron MOP-3 into the mesoporous cages (1.5 nm and 3.8 nm) of Zr-MOF PCN-777 by Lee *et al.*[73]

Recently, Fajal *et al.*[74] developed a unique anion exchangeable composite material (NH_2-MOP@MOA), which was synthesized and shaped by encapsulating the cationic NH_2-MOP, $\{[Cp_3Zr_3O(OH)_3]_4(NH_2\text{-}BDC)_6\}\cdot Cl_4$, (*cf.* Fig. 2n) inside a hierarchically porous metal–organic aerogel (MOA) *via* the "bottle-around-ship" synthesis (Fig. 15). Specifically, NH_2-MOPs, aluminum nitrate and benzene-1,3,5-tricarboxylic acid were well mixed in an aqueous DMF solution, then heated to afford the composite gel-type material (NH_2-MOP@MOG), which was carefully dried under a supercritical CO_2 drying procedure to give the final cationic aerogel material. NH_2-MOP@MOA was proven to have hierarchical porosity with large macropores (>50 nm), mesopores (2–50 nm) and micropores (<2 nm), with the presence of Zr^{IV}-SBUs, free NH_2 groups and exchangeable Cl^- ions in the monolithic aerogel material.

So far, the "bottle-around-ship" and impregnation synthesis of MOP@MOF is still challenging due to the limited stability and solubility of most MOPs. Although "ship-in-bottle" synthesis can avoid the problems, it is difficult to characterize and confirm the position of the assembled MOP in the MOF matrix.

4.8 Enzyme@MOF materials

Enzymes play a vital role in biological processes and industrial production. However, the structural complexity and vulnerability limit their applications in the extracellular environment. Encapsulation of enzyme@MOF has been developed to shield enzymes

from deactivating reaction conditions (*e.g.*, elevated temperatures, and denaturants) and advance reusability and catalytic performances.[1] MOF can provide a hydrophilic/hydrophobic microenvironment around the enzyme and mass transfer channels for the reactants/products during the enzymatic reactions; therefore, the MOF with proper pore size and stability should be judiciously chosen. Depending on whether the MOF is presynthesized or *in-situ* constructed, enzyme@MOF is obtained *via* ''impregnation'' and ''bottle-around-ship'' synthesis, respectively. The former is also called ''pore encapsulation'' or ''pore infiltration''.

Pisklak *et al.*[75] conducted pioneering work to encapsulate the microperoxidase MP-11 into a Cu-based MOF with a channel pore of 1.78 nm and found that MP-11@Cu-MOF greatly promoted the methylene blue oxidation process than free enzyme. Ma *et al.*[76] used a terbium MOF with abundant mesopores (Tb-mesoMOF; 3.9 nm and 4.7 nm) to encapsulate MP-11. As the cavities of Tb-mesoMOF are slightly larger than the size of MP-11, MP-11@Tb-mesoMOF exhibits high loading ability and eye-catching catalytic capacity and recyclability. These promising results have fuelled the interest of researchers in this field. Thanks to the dynamic hierarchical structures of enzymes, the pore infiltration can be an interactive absorption. This was exemplified by the significant conformational change of cytochrome *c* (Cyt *c*) during the enzyme infiltration into the Tb-mesoMOF, which has sufficient pore cavities for Cyt *c*, but the window apertures (1.3 and 1.7 nm) are narrower than that of the enzymes ($\sim$2.6 nm $\times$ 3.2 nm $\times$ 3.3 nm).[77] Cyt *c* adopted a configuration that was different from either denatured or normal enzyme, allowing the entrance of the enzyme. Partial unfolding of the protein structure could also facilitate the encapsulation of protease in MIL-101-NH_2.[78]

MOFs with tunable large pore sizes (meso- and macro-pores) and adjustable environments are important for the impregnation synthesis of enzyme@MOF materials. The Zhou group[79] used large linkers and *in situ* formed super tetrahedral units in MOFs to create ultra-large mesopores (5.50 nm and 4.20 nm) to encapsulate enzymes of different sizes *via* impregnation. Three enzymes with different sizes, namely horseradish peroxidase (HRP, 4.0 nm $\times$ 4.4 nm $\times$ 6.8 nm), Cyt *c* (2.6 nm $\times$ 3.2 nm $\times$ 3.3 nm) and MP-11 (1.1 nm $\times$ 1.7 nm $\times$ 3.3 nm) could occupy the mesoporous cages of PCN-333(Al) with record-high loadings in single-enzyme encapsulation or multiple-enzyme encapsulation manner (Fig. 16). The Farha group[80] compared the catalytic performance of cutinase encapsulated into the mesopores of hierarchically mesoporous NU-1000 and mesoporous PCN-600 with similar pore sizes, and confirmed the important role of hierarchical pore structuring for greater accessibility and higher activity of enzymes and reactant/product diffusion. The encapsulation of HRP and glucose oxidase (GOx) within the large pores of PCN-888 has afforded a nanoscale tandem bioreactor.[81]

When the window apertures of MOFs are smaller than the scale of enzymes, the immobilization of the enzyme within the superstructure of *in situ* formed MOF, also called ''bottle-around-ship'' synthesis, would be more efficient. The bottle-around-ship synthesis can be divided into coprecipitation and biomimetic mineralization (Fig. 17),[82] of which the former needs additive chemicals while the latter not. The initial work of the coprecipitation approach was done by the Liu group,[83] where a mixture of 2-methylimidazole, zinc ions, polyvinylpyrrolidone (PVP), and Cyt *c* gave the Cyt *c*@ZIF-8 (Fig. 17, top).

The Doonan group[84] utilized coprecipitation to tune the hydrophilicity of the environment of the MOF by utilizing ZIF-8, ZIF-90, and MAF-7 (MAF = metal-azolate framework) with micropores to load fluorescein-tagged catalase (FCAT, 4.4 nm $\times$ 4.9 nm $\times$ 5.6 nm) (Fig. 18a). They found that the hydrophobic environment of ZIF-8 can lead to unwanted conformational change and aggregation of enzymes, thereby decreasing its activity, while other two biocomposites with hydrophilic environment showed good decomposing effect on hydrogen peroxide. Another case study was reported by Li *et al.*,[85] who coprecipitated *Burkholderia cepacia* lipase (BCL) and MTV-ZIF-8 with continuously tuned hydrophilicity in the pores that a specific sequence of arrangement could regulate the switch of enzyme conformation (Fig. 18b). The microenvironment effects in MOFs are crucial to the catalytic performances (including activity, stability and selectivity) *via* coprecipitation for enzyme@MOFs. These examples include

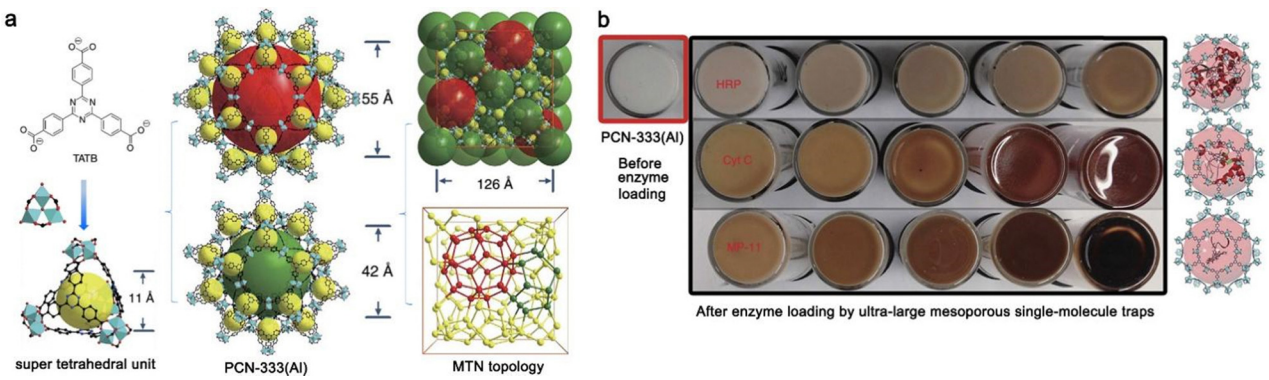

Fig. 16 (a) Structure illustrations of PCN-333(Al); (b) Color variations of PCN-333(Al) when loaded with enzymes (top-down: HRP, Cyt *c*, MP-11) in the mesoporous cages as single-molecule traps at different concentrations. Reproduced from ref. 79 with permission of Nature Publishing Group, Copyright 2015.

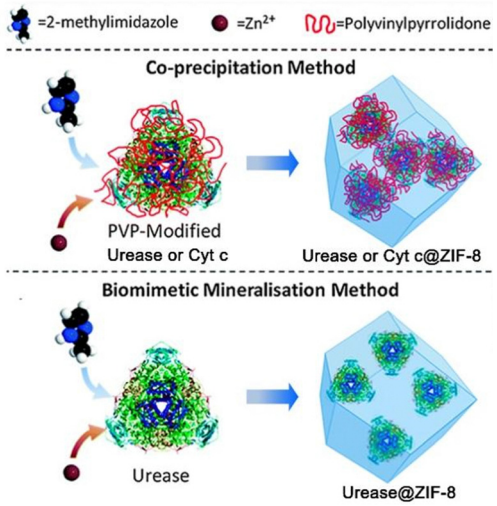

Fig. 17 Schematic view showing coprecipitation in the presence of a capping agent (PVP), and biomineralization *via* "bottle-around-ship" synthesis to immobilize urease or Cyt *c* in ZIF-8. Adapted from ref. 82 with permission of the Royal Society of Chemistry, Copyright 2016.

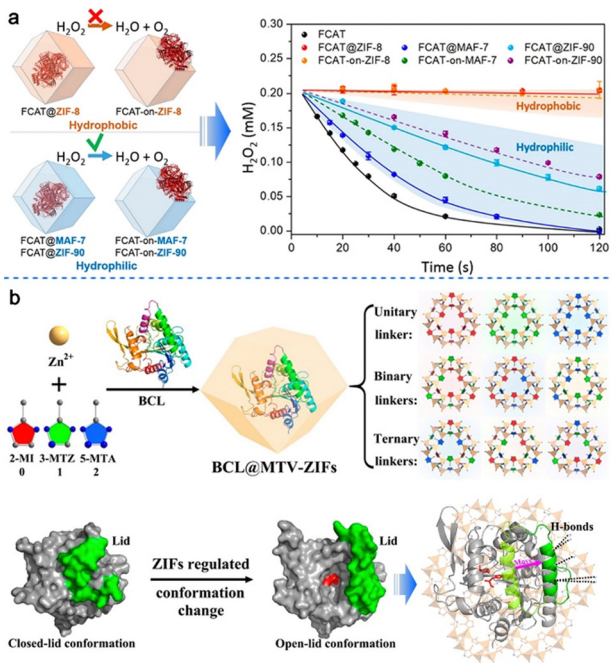

Fig. 18 (a) Schematic views of the FCAT entrapped by a ZIF with different hydrophilicity and the bioactivities of the resulting FCAT@ZIF. Reproduced from ref. 84 with permission of the American Chemical Society, Copyright 2019. (b) One-pot-synthesis of BCL@MTV-ZIFs, in which the closed-lid/open-lid conformation of BCL was regulated by MTV-ZIFs. Reproduced from ref. 85 with permission of the American Chemical Society, Copyright 2021.

Cyt *c*@NKMOF-101-Zn by the Chen group,[86] α-glucosidase α-G/GOx@Cu-MOF by the Zhao group,[87] and *Candida rugosa* lipase (CRL)@ZIF-8 by the Luo group.[88]

Biomimetic mineralization represents another efficient approach to construct biocomposites with enzymes as seeds

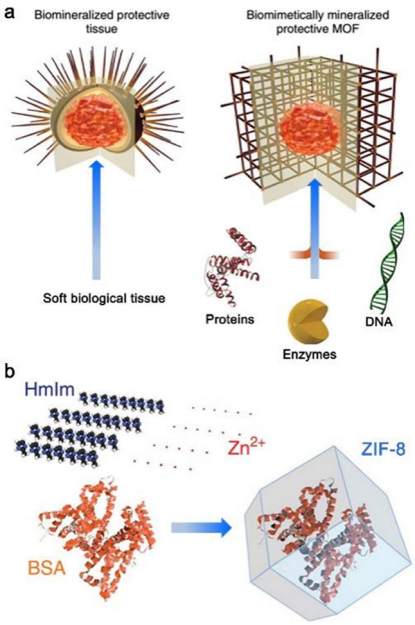

Fig. 19 (a) Schematic view of a hard porous protective shell of a sea urchin that is biomineralized by soft biological tissue and the biomimetically mineralized MOFs; (b) *in situ* encapsulation of the BSA within ZIF-8 *via* biomineralization processes. Reprinted from ref. 89 with permission of Nature Publishing Group, copyright 2015.

for the construction of MOF coatings in the absence of facilitators. Various biomacromolecules (such as proteins, enzymes and DNA) have been "mineralized" into MOFs first by the Falcaro group (Fig. 19).[89,90] During the synthesis, the enzymes inside could modulate the crystal size, morphology and crystallinity, which in turn generate new cavities that tightly surround the enzymes and form strong interactions with the enzymes inside concomitantly. The Shieh group[91] demonstrated that the robust yet size-matched window of MOF for accommodating the catalase allowed for increased recyclability and stability.

Some excellent review articles on enzyme@MOF materials are recommended for their insights and comprehensiveness. These review articles are focused on the strategies to immobilize enzymes,[92] the mesopores,[93] microenvironment,[42] and key advantages of MOFs[94] for enzyme encapsulation; and multi-enzyme systems[95] *via* MOFs for cascade reactions, and MOF/enzyme-based biosensors.[96]

5. Applications: enhancement in performance of host@MOF materials

With the expectation that host@MOF and guest@host@MOF should combine the advantages of host or guest@host and MOFs in specific applications, many efforts have been devoted to this area. The host@MOF materials provide a unique way not only to control the environment of host molecules in the solid state but also to change the properties of MOFs.[61] This section briefly summarizes the various applications of host@MOF materials in gas sorption and separation, environmental

remediation, heterogeneous catalysis, ion conduction and proton conduction.

5.1 Gas sorption and separation

The increasing carbon dioxide (CO_2) concentration in the atmosphere causes a series of environmental problems. Sulfur dioxide (SO_2) is responsible for the formation of 'acid rain' that poses a significant danger to the health of ecosystems.[97] The selective CO_2 and SO_2 removal from fuel gases and post-combustion gases are imperative for a sustainable development. Adsorptive separation is seen as a technique for the capture of trace amounts from industrial gas streams. A lot of sorbents,[98] including cages[99] and MOFs,[100] and their composites have been evaluated for CO_2 or SO_2 removal with promising results.

Liang *et al.*[25] reported that the composite CB6@MIL-101-36 (36 wt% of CB6, *cf.* Fig. 12) exhibited higher CO_2 uptake capacities of 79 $cm^3\ g^{-1}$ than CB6 and MIL-101 (37 and 44 $cm^3\ g^{-1}$, respectively) at 1 bar due to more adsorption sites associated with CB6 in the composite. The CB6@MIL-101 composites also exhibited an increased CO_2/CH_4 selectivity for a $CO_2:CH_4$ mixture (2 : 98) at 1 bar over the individual components. This was confirmed by the gas separation results conducted on mixed-matrix membranes (MMMs) of 16 wt% CB6, MIL-101 or CB6@MIL-101-36 in Matrimid as the continuous polymer matrix (Fig. 20). Therefore, encasing CB6 cages in the pores of MIL-101 enhanced the CO_2/CH_4 selectivity to ~47 without significant decrease of permeability compared with MIL-101 at low pressures (Fig. 20b).

Zhang *et al.*[49] found that Cd@TMPyP@MOM-11(Cd) (Fig. S1, ESI†) modified with metal chloride salts (*e.g.* $MnCl_2$) exhibited higher volumetric CO_2 uptake, and enhanced CO_2/CH_4 selectivity than the parent Cd@TMPyP@MOM-11(Cd) due to enhanced interactions with CO_2.

Liang *et al.*[99] reported that a CB6-based HOF material (nanoCB6-H) shows a relatively high SO_2 uptake capacity, a high SO_2/CO_2 selectivity of 120, and an outstanding cycling performance for dry SO_2. The adsorption sites on CB6 were revealed by FT-IR and DFT calculations. However, the nanoCB6-H was not stable under humid SO_2 conditions, which might hamper its practical applications. Later, Sun *et al.*[70] embedded CB6 in MIL-101 to obtain CB6@MIL-101-Cl-31 (with 31 wt% of CB6, *cf.* Fig. 12), which showed an impressive record for SO_2 uptake of 19.5 mmol g^{-1} at 1 bar and 293 K due to the combined merits of CB6 cages with high affinity towards SO_2 and MIL-101 with high SO_2 uptake capacity (Fig. S3, ESI†). Notably, CB6@MIL-101-Cl exhibited enhanced chemical stability under the exposure to both dry and humid SO_2.

Recently, Zhang *et al.*[61] successfully transformed the still slightly flexible structure of ZIF-8 to a rigid structure by encapsulating B15C5 in the nanopores (*cf.* Fig. 9). Impressively, compared with ZIF-8, the B15C5@ZIF-8 membranes exhibited a doubling in C_3H_6/C_3H_8 selectivity to approx. 220, outperforming state-of-the-art membranes. Moreover, B15C5@ZIF-8 membranes manifested an unusual positive increase in the C_3H_6/C_3H_8 separation factor with elevated pressure, achieving a record-high C_3H_6/C_3H_8 separation factor of 331 under 7 bar. Theoretical simulation revealed that the rigid pore window of B15C5@ZIF-8 poses a higher diffusion energy barrier for C_3H_8, resulting in improved C_3H_6/C_3H_8 kinetic selectivity. This simple strategy might inspire more work to improve the gas separation performance of flexible microporous MOFs.

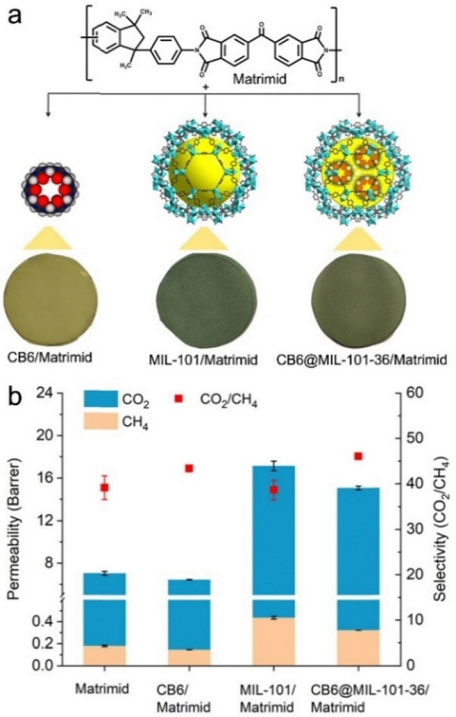

Fig. 20 (a) Schematic views of the structure of Matrimid (top), the porous fillers (middle), and the mixed matrix membranes (bottom). (b) Performance of Matrimid membrane, CB6/Matrimid, MIL-101/Matrimid, and CB6@MIL-101-36/Matrimid membranes with a loading 16 wt% for the separation of CO_2 from a 50 : 50 v : v CO_2/CH_4 mixture at 25 °C and 3 bar. Reproduced from ref. 25 with permission of Wiley-VCH Verlag GmbH & Co., Copyright 2020.

5.2 Environmental remediation

Water contamination by heavy metals, such as As(v) and Pb(II), and their detrimental effects on human health and the environment have been a worldwide concern.[101] The Environment Protection Agency (EPA) lists metal-based oxoanions as potential toxic inorganic pollutants in wastewater.[102] The efficient removal of these pollutants is an urgent topic. Adsorption is one of the most feasible and cost-effective methods for treating wastewater.

Liang *et al.*[39] reported the adsorbent MC5@MIL-100(Fe)-23 (23 wt% of MC5, *cf.* Fig. 13) with reversible Pb^{2+} removal capability, enhanced and selective adsorption performance (Fig. 21). They observed faster uptake kinetics (0.239 *versus* 0.094 g $mg^{-1}\ min^{-1}$) and higher removal efficiency (99.7% *versus* 53%) for Pb^{2+} by MC5@MIL-100(Fe)-23 than by MIL-100(Fe). The encapsulated MC5 molecules as active domains possess relatively high affinity toward Pd^{2+} ions, thus show selective Pb^{2+} removal in the presence of other mineral ions

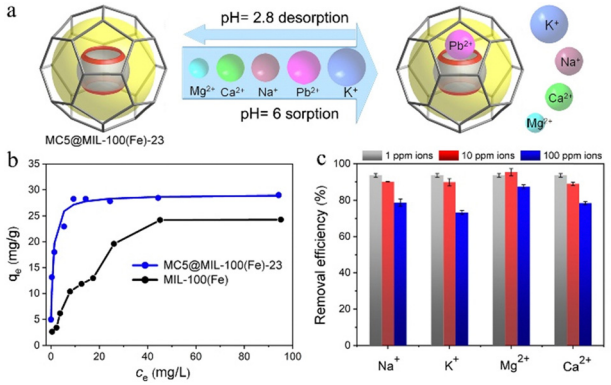

Fig. 21 (a) Schematic view of selective capture of Pb^{2+} by MC5@MIL-100(Fe)-23 among other mineral cations in water. (b) Pb^{2+} adsorption isotherms by MC5@MIL-100(Fe)-23 and MIL-100(Fe). (c) The effects of coexisting ions on the removal efficiency of Pb^{2+} at 1 mg L^{-1} (1 ppm) by MC5@MIL-100(Fe)-23. Reprinted from ref. 39 with permission of Wiley-VCH Verlag GmbH & Co., Copyright 2021.

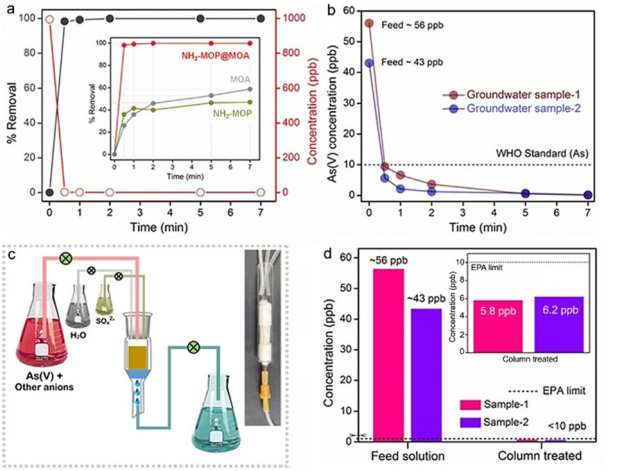

Fig. 22 (a) Sorption kinetics study of low concentration (1 ppm) of $HAsO_4^{2-}$ by NH_2-MOP@MOA (inset: comparison between NH_2-MOP@MOA and pristine materials). (b) Arsenic removal results on natural ground water samples. (c) Schematic diagram of the dynamic column-exchange-based As^V adsorption experiment. (d) Result of dynamic sorption-based recyclable As^V capture. Reproduced from ref. 74 with permission of Wiley-VCH Verlag GmbH & Co., Copyright 2022.

(Na^+, K^+, Mg^{2+}, and Ca^{2+}) (Fig. 21c). This was explained by the size matching effect between the MC5 portal size of 2.5 Å and the Pb^{2+} ion size of 2.4 Å. The selective binding of Pb^{2+} to the carbonyl groups of MC5 in the composite was demonstrated by the FT-IR spectra shift and X-ray photoelectron spectroscopy (XPS) analysis. However, only about one sixth of the amount of encapsulated MC5 cages were used as the adsorption domains and most of them were probably blocked.

Fajal *et al.*[74] reported an ionic aerogel material denoted as NH_2-MOP@MOA (*cf.* Fig. 15). NH_2-MOP@MOA shows highly selective and very fast removal efficiency (>80% at 50 ppm) for hazardous oxoanions such as $HAsO_4^{2-}$, SeO_4^{2-}, CrO_4^{2-}, MnO_4^-, and ReO_4^- in water. Notably, NH_2-MOP@MOA could selectively remove trace $HAsO_4^{2-}$ at a very low concentration (≈1 ppm) in the presence of ≈100-fold of interfering anions, while the neat NH_2-MOP and MOA showed relatively less selective capture efficiencies (Fig. 22a). Moreover, NH_2-MOP@MOA demonstrated rapid elimination of As^V to far below the WHO set levels (10 ppb) in 1 min (Fig. 22b). In flow-through adsorption experiments using a NH_2-MOP@MOA packed column, the level of As^V in toxic natural drinking water sample was reduced to far below the EPA permitted limit (10 ppb) (Fig. 22c and d). Such excellent selective sorption capability results from the cooperative effect of the large macropores along with high surface area, the presence of free $-NH_2$ groups and exchangeable Cl^- ions inside NH_2-MOP@MOA.

5.3 Heterogeneous catalysis

Homogeneous catalysts including metalloporphyrins,[103] metallophthalocyanines,[53] metal–organic polyhedrons,[71] and enzymes[2] have widespread applications. However, many homogeneous catalysts suffer from limited life time activity due to degradation and the problem of catalyst separation and reuse. Encasing active species in porous matrices is a promising approach to circumvent these issues. Recent years have witnessed the applications of host@MOF and guest@host@MOF materials in some representative organic reactions (Fig. S4, ESI†) and enzymatic reactions.

5.3.1 Hydrocarbon oxidation. For cyclohexane oxidation (Fig. S4a, ESI†), Alkordi *et al.*[44] investigated Mn@TMPyP@MOM-2 (*cf.* Fig. 4) as a recyclable catalyst in the presence of *tert*-butyl hydroperoxide (*t*BuOOH) as an oxidant. A total yield (from cyclohexane to cyclohexanol/cyclohexanone) of 91.5% and a corresponding turn over number (TON) of 23.5 were observed, while TMPyP@MOM-2 and MOM-2 were not active, suggesting Mn@TMPyP as the active site.

For the tetralin oxidation (Fig. S4b, ESI†), Kockrick *et al.*[54] showed that Fe@PcF_{16}@MIL-101 and Ru@PcF_{16}@MIL-101 (*cf.* Fig. 2b, bottom) have very high TONs with 48 200 and 46 300 after 24 h, which was higher than for the homogeneous counterpart catalyst (*e.g.* Fe@PcF_{16}, TON = 6300) due to the confinement in the pores which prevented the deactivating dimerization.

For the selective oxidation of benzyl alcohol to benzaldehyde (Fig. S4c, ESI†), M_6L_4@MIL-101(Cr) developed by Qiu *et al.* (*cf.* Fig. 14)[34] gave a 98% selectivity to benzaldehyde at 95% conversion. It is impressive that the yield was enhanced by a factor of *ca.* 3.5 over free M_6L_4. Moreover, the catalytic activity and selectivity of M_6L_4@MIL-101(Cr) remained almost unchanged after five reuses, while the free M_6L_4 deactivated dramatically. The remarkably enhanced performance of M_6L_4@MIL-101(Cr) was explained by the encapsulation effect, which hampered the deactivation of M_6L_4 active centers.

5.3.2 Olefin oxidation. Zhang *et al.*[47] evaluated the olefin oxidation capability of Fe@TMPyP@MOM-4(Fe) (*cf.* Table S1, ESI†), which showed enhanced conversion in the oxidation of styrene (4.2 Å × 7.0 Å cross section) to styrene oxide and benzaldehyde than Fe(III)@TMPyP in solution (Fig. S4d, ESI†), and size selective catalysis since much lower activities were

obtained when *trans*-stilbene (4.2 Å ×11.4 Å cross section) was used as the substrate, which is larger than the pores (~9 Å × 9 Å) of the MOF. The epoxidation of *trans*-stilbene (Fig. S4e, ESI†) could also be catalysed by Mn@TMPyP@MOM-10(Mn)[48] (*cf.* Table S1, ESI†). Li *et al.*[55] proved Co@Pc@bio-MOF-1 (*cf.* Fig. 6) as an active and stable catalyst for styrene epoxidation reaction, with a higher conversion (72%) and selectivity (65%) than the homogeneous Co@Pc catalyst (38% conv., 60% select.) and bio-MOF-1 (8% conv.), highlighting the advantage of confinement effect. For the same reaction, Yegneh *et al.*[57] found that Cu@Pc@MIL101(Cr) exhibited enhanced catalytic performance with 100% conversion and 85% selectivity to styrene oxide due to high surface area and the presence of catalytic active sites of both MIL101(Cr) and encapsulated Cu@Pc, with O_2 as oxidant.

5.3.3 Cyclic addition. Ionic metalloporphyrins containing Lewis acid–base pairs can be confined in MOFs to provide catalysts for the cyclic addition reaction of CO_2 with epoxide substrates (Fig. S4f, ESI†). Mn@TMPyP@ZIF-8 efficiently converted CO_2 into cyclic carbonates.[50] Zn@TMPyP@PCN-224 was also a good catalyst for this reaction.[51] The promising catalytic performances were explained by the synergistic effect between the MOF (for CO_2 enrichment) and ionic metalloporphyrins (Lewis-acid metal sites and I^- ions for epoxide activation and conversion). Guest@host@MOF materials with mesopores should be more attractive for promoting this reaction under mild conditions.

5.3.4 Oxidative amidation. Oxidative amidation of aldehydes with amines offers green and significant protocols for the construction of amides due to the stability and availability of the starting materials. Boroujeni *et al.*[56] demonstrated that Cu@Pc@MIL-101 showed enhanced catalytic yield (92%) than Cu@Pc (10%) and MIL-101 (35%) for the product *N*-benzylbenzamide (Fig. S4g, ESI†). Fairly good to excellent yields of amides were obtained from a wide range of benzaldehydes.

5.3.5 Biocatalysis of enzyme@MOF. The enzymatic reactions of enzyme@MOF materials can be divided into several types based on the reaction enzyme catalyses, including hydrolysis, oxidation, peroxide degradation, and cascade reactions.

Hydrolysis refers to breaking substrates into smaller molecules with hydrolase. The Falcaro group[89] did pioneering work of imbedding urease in ZIF-8 for enhanced performance in decomposing urea to ammonia and carboxylate. The encapsulated organophosphorus acid anhydrolase (OPAA) in PCN-128y exhibited higher thermal stability than free OPAA and comparably high conversion (80–90%) for the hydrolytic degradation of the chemical warfare agent soman (Fig. 23).[104] By taking advantage of β-glucosidase for polysaccharides hydrolysis, β-G@Cu(PABA) displayed high efficacy for degrading cellulose to glucose.[105] The biocomposite could work for hours due to the good stability of Cu(PABA) toward acids in pH = 5. Thus, the catalytic properties of enzymes and high stability of porous MOFs are combined in these composites.

Oxidoreductases, such as HRP, GOx and Cyt *c*, are extremely important for redox chemistry. The Falcaro group[89] has immobilized HRP in ZIF-8 *via* the biomineralization path to

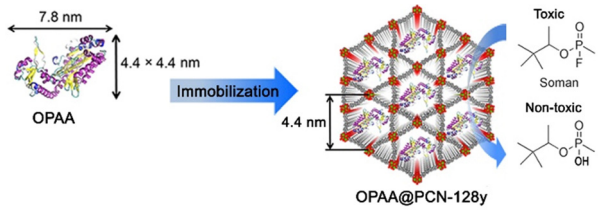

Fig. 23 Hydrolysis reaction for chemical warfare agent degradation using OPAA encapsulated in the mesoporous channels of PCN-128y. Adapted from ref. 104 with permission of the American Chemical Society, Copyright 2016.

catalyse the reaction of pyrogallol to purpurogallin. It was surprising that the catalytic activity of encapsulated HRP sustained more than 80% even in boiling water and DMF. GOx and Cyt *c* could also be immobilized in MOFs *via* a similar method by the Ouyang group.[106] The chosen MOFs with small windows could strengthen the stability of enzyme@MOF materials, but also hampered the diffusion of reactants/products through the pores.

Catalase is frequently immobilized to show enhanced stability toward H_2O_2 degradation. The Tsung group[90] embedded catalase in ZIF-90 *via* a coprecipitation path, and the hydrophilic environment around catalase enabled the stabilization from protease. A hierarchically porous hollow ZIF-8 framework was used as a host to offer freestanding movements of the enzyme catalase, resulting in nearly 3-fold activity of the confined enzyme.[91]

Cascade reactions can be possible when multiple enzymes are immobilized in the MOF matrices. GOx and HRP were coprecipitated into ZIF-8 by the Ge group under mild conditions.[107] The biocomposite achieved the cascade reaction from glucose to gluconic acid and H_2O_2, while at the same time, HRP consumed H_2O_2 to oxidize $ABTS^{2-}$ (Fig. 24). The biocomposite showed recyclability, substrate selectivity and sustains 80% of the original ability after 7 days. Recently, two enzymes FateDH and FaldDH and porphyrin were encapsulated in ZIF-8 to form a cascade bioreactor that converted CO_2 to formaldehyde with light irradiation.[108] The Lv group[109]

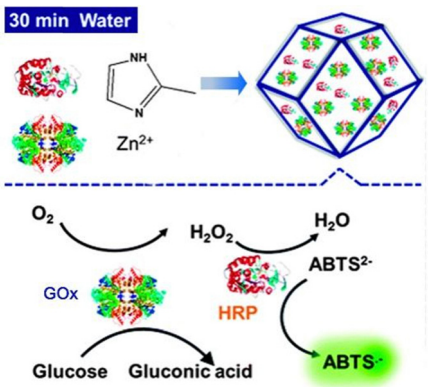

Fig. 24 GOx and HRP-contained ZIF-8 that performed the oxidation of glucose and electron transport to water. Reproduced from ref. 107 with permission of the Royal Society of Chemistry, Copyright 2015.

developed a core-shells strategy to construct a complicated MOF matrix, where NH_2-MIL-101(Cr) was the core and two layers of HKUST-1(Cu) were the shells. This special system reduced CO_2 to formate *via* the encapsulated three-enzyme cascade system consisting of carbonic anhydrase, formaldehyde dehydrogenase, and glutamate dehydrogenase.

Considering the diversity of enzymes and facile syntheses of MOF matrices, biocomposites based on single enzyme@MOF and multiple enzymes@MOF are emerging for various biocatalytic reactions. Since enzymes usually possess nanoscale sizes and most of the chosen MOFs contain micropores, enzymes are often encapsulated in the superstructures of the MOF *via* a "bottle-around-ship" synthesis. It remains a big challenge to precisely locate an enzyme in the MOF crystallite and achieve synergistic catalysis. Besides, improving the enzyme activity, selectivity, and stability, and operating enzyme@MOF materials under industrial conditions should be the goal for this direction. Therefore, there is much work to do including increasing the enzyme loading amount, tuning the framework-enzyme interactions, large-scale synthesis, *etc.*

5.4 Ion conduction

Inspired by the exquisite ion selectivity of biological Na^+ channels in living systems, the construction of artificial ion channels has been a hot spot and active area due to the vital role of ion transport in diverse fields from separation to energy conversion. Since the first example by Ma *et al.*[58] to encapsulate crown ethers (18C6) in microporous ZIFs for the construction of artificial ion channels, continuing efforts are devoted to CE@MOF materials for ion selective transport.

Ma *et al.*[58] found that the 18C6 modified pores of ZIF-67/ZIF-8 can act as selective filters and provide specific coordination with K^+ ions but relatively weak coordination ability to Na^+ and Li^+. Thus, both the Li^+ conductivity (1.46×10^{-2} S cm^{-1}) and selectivity for Li^+/K^+ (9.5) and Na^+/K^+ (6.4) were higher than for ZIFs without 18C6 (7.68×10^{-3} S cm^{-1}, 2.8, 1.7, respectively).

Li *et al.*[59] used the larger benzo-12-crown-4-ether (BCE) and anionic ZIF-7 to fabricate M@BCE@ZIF-7 (M = Li^+, Mg^{2+}, Al^{3+}) (*cf.* Fig. 7) with tunable channel charges for selective ion transport. A very high Li^+/Mg^{2+} selectivity of *ca.* 125 was achieved in the positively charged membrane (Al^{3+}@BCE@ZIF-7). Mechanistic studies suggested that the positively charged channel increased the entry energy of cations, and enlarged the energy barrier difference between Li^+ and Mg^{2+}, leading to obviously enhanced Li^+/Mg^{2+} selectivity (*cf.* Fig. 7b). In the M@BCE@ZIF-7 membrane, electrostatic repulsion interactions of M@BCE and a size screening effect of ZIF-7 were combined to promote selective ion transport.

Xu *et al.*[60] further loaded the dibenzo-crown ethers DB15C5 or DB18C6 in UiO-66 with a window size of ~8 Å to obtain DB15C5@UiO-66 and DB18C6@UiO-66 membranes (*cf.* Fig. 8). It was demonstrated that the channel of these CE@UiO-66 membranes would promote the transport of monovalent ions, while block divalent ions when the monovalent ion coexists with the divalent ion, thus achieving a significantly higher K^+/Mg^{2+} selectivity of 57 than that (13) of a neat UiO-66 membrane Therefore, the pore size sieving effect of UiO-66 and the interaction screening effect of the CE cavity were important for the enhanced performance.

5.5 Proton conduction

High proton conductivity of solid electrolytes (such as MOFs) is important in proton exchange membrane fuel cells. The key to improving the proton conductivity of MOF is to construct efficient proton transfer channels. NH_2-MOP@DUT-68 (Fig. S2, ESI†)[72] showed enhanced proton conductivity of 1.14×10^{-3} S cm^{-1} than that of DUT-68 (8.83×10^{-6} S cm^{-1}) under the same conditions. It is proposed that hydroxyl groups in the $Zr_6O_6(OH)_2$ nodes of DUT-68, the amino groups on MOP and water molecules are all responsible for the successive hydrogen bonded network to realize the proton hopping. Lee *et al.*[73] demonstrated that MOP-3@PCN-777 showed four orders of magnitude higher proton conductivity of 2.11×10^{-4} S cm^{-1} than 5.69×10^{-8} S cm^{-1} for PCN-777.

5.6 Biosensing

Host@MOF materials can be designed to be desirable candidates for biosensors. Biosensors based on enzyme@MOF materials have been developed to combine the good specificity of enzymes and multiple functions of MOFs, thus strengthening MOFs in the biosensor realm during the last few years.[110–118]

Zhang *et al.*[110] reported a GOx@ZIF-8 modified Au electrode biosensor, which exhibited satisfactory sensitivity, superior stability, selectivity and feasibility for the detection of glucose. ZIF-8 acted as a rigid protective shell and analyte collector, while glucose was catalyzed by GOx to produce H_2O_2, which was electrochemically oxidized on the electrode to output the amperometric response. GOx@ZIF-8 modified long period grating (LPG) was used as a label-free optical fiber biosensor for the detection of glucose with concentration from 1 to 8 mmol L^{-1} with a sensitivity of about 0.5 nm/(mmol L^{-1}).[111] To solve the problem of enzyme leaching and improve control on enzyme location, GOx and HRP crosslinked by a rationally designed DNA scaffold were encapsulated into ZIF-8 as a multi-enzyme (GOx/HRP@DNA@ZIF-8) biosensor system for glucose detection by Song *et al.*[112] The combination of oxygen-related GOx and the luminescent oxygen-sensitive MOF Cu-MAF-2 led to a multifunctional GOx@MAF-2 material with a long stability and heat resistance. This GOx@MAF-2 biosensor could detect glucose with a limit of 1.4 μmol L^{-1}.[113] Wang *et al.*[114] reported the field-effect transistor sensor with bimetallic Ni/Cu-MOF loaded glucose oxidase (GOD), which displayed a piecewise linear relationship in the wide range (1 μmol L^{-1}–20 mmol L^{-1}) and a low detection limit (0.51 μmol L^{-1}) of glucose.

Single/multiple enzymes encapsulated into microporous ZIF-8 provided a portable MOF paper in which cascade reactions can occur to detect glucose and uric acid assisted by smartphone colorimetry.[115] A peptide functionalized HRP@ZIF-90 biosensor was fabricated to detect secreted protein acidic and rich in cysteine (SPARC) (Fig. 25).[116] The peptide sequence was designed to recognize and bind SPARC, while

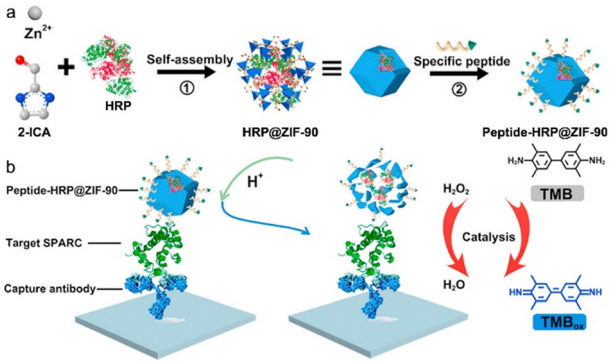

Fig. 25 Schematic diagram for (a) the fabrication process of Peptide-HRP@ZIF-90 and (b) colorimetric detection of target SPARC. Reproduced from ref. 116 with permission of Elsevier B.V., Copyright 2022.

HRP released from the acid-unstable ZIF-90 catalysed the chromogenic reaction, achieving the ultrasensitive SPARC detection with a low detection limit of 30 fg mL^{-1}. Mesoporous carbon spheres/UiO-66-NH_2 with embedded laccase exhibited superior activity and enhanced stability as compared with the free Lac enzyme due to the mesoporous structure and good conductivity of the composite. The biosensor exhibited a detection range of 1.0×10^{-6}–6.0×10^{-5} mol L^{-1} and a relatively low detection limit of 8.94×10^{-7} mol L^{-1} for tetracycline detection.[117] Hydrophilic MAF-7 encapsulated Cas12a nuclease *via* impregnation and displayed enhanced salt, heat and organic solvent tolerance over free nuclease, achieving an ultrasensitive detection limit of 1 copy of SARS-CoV-2 RNA.[118]

So far, most enzyme@MOF based biosensors are based on microporous MOFs (such as ZIF-8, ZIF-90) with small window sizes, and the analyte is focused on the accurate detection of glucose for the diagnosis of diabetes. Most of these biosensors exhibited elevated stabilities and tolerance as compared to free enzymes. More mesoporous MOFs could be used to fabricate host@MOF biosensors and devices for more types of analytes with the goal of high detection sensitivity, selectivity and stability.

6. Characterization techniques

To investigate the structural compositions and porosities of host-in-host materials, some useful characterization techniques are summarized.

6.1. X-ray diffraction techniques

The most widely used X-ray techniques include single crystal diffraction and powder X-ray diffraction (PXRD).[119] X-ray crystallography is a method to determine the arrangement of atoms, host molecules within a single crystal[49,65] with good quality and proper crystal size. The PXRD patterns are also extensively used to determine the crystalline structures and to verify the phase identity of MOFs and host@MOF materials.[39]

6.2. Infrared (IR) spectroscopy

IR is a simple reliable technique widely used to characterize the formation of host@MOF materials as it can provide insights into the presence of chemical groups of the composite material and on the chemical interactions between host molecules and MOFs.[25] It is convenient to conduct *in situ* IR to investigate the interactions of host@MOF materials towards specific guest molecules.

6.3. Ultraviolet-visible (UV-vis) spectroscopy

UV-vis spectra refer to absorption spectroscopy or reflectance spectroscopy in the ultraviolet-visible spectral region. UV-vis absorption is useful to give structural information when the host molecules or MOFs can absorb the energy in the form of ultraviolet or visible light to excite electrons from the ground state to the excited state. For example, porphyrin chromophore usually shows one Soret band adsorption, and four Q bands, while metalloporphyrins show one Soret band and two predominant Q bands due to higher symmetry after metal coordination.[120]

6.4. Nuclear magnetic resonance (NMR) spectroscopy

Solution ^{1}H NMR spectra are useful to conduct a qualitative and quantitative analysis of host molecules after digestive dissolution of the host@MOF composite.[25,58,61] Solid state ^{13}C NMR spectra can give information on host molecules, and the interactions between encapsulated molecules and MOFs.[34]

6.5. Elemental analysis (EA)

Metal analysis using atomic absorption spectroscopy (AAS) or inductively coupled plasma-atomic emission or mass spectrometry (ICP-AES, ICP-MS) can be used to calculate the metal content in the host@MOF materials. Energy dispersive X-ray (EDX) spectroscopy element mapping at nanometer resolution can be used to investigate the dispersion and quantity of elements near the surfaces of host@MOFs.[34] Moreover, X-ray photoelectron spectroscopy (XPS) can be a standard method to determine the valence state and molar ratio of metal centers near the surfaces (normally within 10 nm).[121]

6.6. Gas sorption

N_2 (or argon) adsorption is the standard technique to evaluate the porosities of framework materials. Encapsulating molecules in the pores of MOFs usually leads to decreased surface areas and narrower pore size. By recording two adsorption isotherms of the same materials at different but close temperatures ($\Delta T \leq 20$ K), the isosteric heat of adsorption (Q_{ads}) or enthalpy of adsorption ($\Delta H_{ads} = -Q_{ads}$) can be determined to describe binding energies for an adsorbate–adsorbent pair.[122] Q_{ads} or ΔH_{ads} are defined as the energy to be released/required when an adsorbate binds to/detaches from the solid surface of an adsorbent.

6.7. X-ray absorption techniques

The synchrotron-based X-ray absorption spectroscopy (XAS) including X-ray absorption near-edge structure (XANES) and extended X-ray absorption fine structure (EXAFS) measurements can be performed to further confirm the local coordination environment of the metal species in host@MOFs.

6.8. Other techniques

Microscopy techniques, such as scanning electron microscopy (SEM) and transmission electron microscopy (TEM), are essential tools to elucidate the morphology of materials. Aberration-corrected high-angle annular dark-field scanning transmission electron microscopy (AC-HAADF-STEM) can provide a resolution high enough to observe molecules at the subnanometer scale. In addition, confocal laser scanning micrographs (CLSM) can be used to assess the spatial distribution of fluorescent host molecules including enzymes within the samples.[84]

7. Conclusions and outlook

During the past decade, a variety of host@MOF materials have been achieved for various applications. The concept and advantages of host@MOF have been established in this review. We have summarized the encapsulation approaches for the construction of host@MOF and guest@host@MOF materials, which mainly include wetness impregnation, bottle-around-ship, and ship-in-bottle synthesis. Subsequently, the syntheses of host@MOF materials based on various types of host molecules are introduced. Then, the enhanced performances of MOFs with encapsulated host molecules and guest@host moieties demonstrate the confinement effects, and synergistic roles of the constituent parts. Some useful characterization techniques to analyse these materials are presented.

Metal–organic frameworks not only serve as ideal supports for various functional host molecules, but also open a door for new composites with enhanced properties due to their infinite structural designability and high surface areas. Despite the impressive success, host@MOF materials are still in their infancy and face challenges but also opportunities in terms of synthesis (i–iii), characterization (iv and v) and applications (vi–ix).

(i) Currently, the types of MOFs for encasing host molecules and guest@host moieties are still limited (Tables S1 and S2, ESI†). Most of these MOFs have relatively small micro-/mesopores (such as ZIF-8, ZIF-67, UiO-66, MIL-101, MIL-100) and simple linkers, which could readily encapsulate the host molecules and allow the diffusion of small substrates, but may not be advantageous for mass transfer of bulky guest species. Based on the hard/soft acid–base concept, stable MOFs can be tailor-made to avoid leaching of encapsulated host molecules (including enzymes). Such stable MOFs with tunable pores, window sizes and rich functional groups should be paid more attention to the construction of host@MOF materials for targeted applications in the future.

(ii) The encapsulated host molecules are mainly limited to enzymes and typical macrocycles, such as porphyrins, phthalocyanines, cucurbiturils and metal–organic polyhedrons, with little attention on other functional host molecules (such as pillararenes, nonheme complexes, imine cages, *etc*). This research gap indicates an opportunity for expanding the families of host@MOF materials if related issues including solubilities, directing capabilities of host molecules are addressed and appropriate synthetic paths are chosen. Multivariate host@MOF materials containing more than one type of host molecules are possible and should be further explored to obtain multifunctional systems in the future.

(iii) Most of the host@MOF and guest@host@MOF composite materials are obtained *via* solvothermal synthesis. Other synthetic methods such as mechanochemical synthesis, microwave-assisted synthesis, microfluid synthesis, and electrochemical synthesis, should also be explored for fast, large-scale synthesis, and possible shaping of host@MOF materials in the future. The use of commercially available host molecules (including enzymes) and easily available MOF precursors should also be pursued.

(iv) So far, it remains a big challenge to get single crystals of host@MOF materials. Only a few porphyrin@MOF and cavitand@MOF materials have been characterized by single crystal X-ray diffraction. Figuring out the position and microenvironment of the host molecule in the MOF matrix would be helpful to disclose the detailed structure–property relationship. The ''bottle-around-ship'' synthesis may form single crystals of host@MOF materials due to the molecular level assembly. Moreover, various characterization techniques should be combined to fully analyse the structures of host@MOFs.

(v) For most cases, the enhanced properties are attributed to the confinement and synergistic effects between the host molecules and the MOF matrix. A deeper understanding of the mechanism at the molecular level would facilitate the designs of task-specific host@MOF materials. Advanced characterization methods and theoretical calculations should be combined to illustrate the potential roles of hierarchical pores, the host molecule and the MOF, and their mutual interactions.

(vi) Most of the host@MOF materials are successfully designed to improve the activity, selectivity and stability of host or guest@host molecules (such as enzymes) for predictable applications. Nevertheless, there is only a limited number of state-of-the-art host@MOF materials available. More attention should be paid to the MOF aspect and synergistic functions brought about by both the host molecule and the MOF in various applications. For example, Zhang *et al.*[61] used the host@MOF strategy to stabilize the flexible ZIF-8, thus achieving the impressive high C_3H_6/C_3H_8 separation performance.

(vii) Some unique host molecules or derived new polymers may be synthesized in the cage-shaped or channel pores of MOFs (as template) because MOFs possess ordered pores and can be degraded to release guest species.[123] This provides new opportunities for synthetic chemistry and materials chemistry in confined space.

(viii) The exploration of catalytic cascade systems by integrating more than two catalytically active species into host@MOF materials deserves more attention in the future. While metal@host@MOF catalysts are predominantly studied as single atom catalysts, novel catalysts with unique properties (*e.g.* synergistic catalysis, tandem catalysis) may be created by exploiting host@MOF materials to stabilize metal clusters.[124]

(ix) More efforts should be made to evaluate the performance of host@MOF and guest@host@MOF materials in target environments, which will further push these materials toward practical applications under industrial conditions, *etc.*

In summary, deriving host@MOF materials *via* encapsulation paths has been an important and evolutional direction. It is a very promising route to construct complex systems with well-defined hierarchical structures. Progress in this fascinating area will certainly lead to more functional materials like guest@host@MOF with more applications by the continuous joint efforts of researchers from supramolecular chemistry, coordination chemistry, catalysis and enzyme chemistry.

Data availability

No primary research results, software or code have been included and no new data were generated or analysed as part of this review.

Conflicts of interest

There are no conflicts to declare.

Acknowledgements

J. L., R. W. and Q. W. acknowledge the financial support from the Natural Science Foundation of Hebei Province (B2021202077, B2022202039, B2024202073), National Natural Science Foundation of China (22001178, 21975259), Postdoctoral Fellowship Program of CPSF (No. GZC20240369) and startup funding from Hebei University of Technology. C. J. thanks the Deutsche Forschungsgemeinschaft (DFG) for funding within the Priority Program SPP 1928/2 COORNETs (C. J. grant Ja466/43-1).

Notes and references

1 K. Wang, J. Zhang, Y. C. Hsu, H. Lin, Z. Han, J. Pang, Z. Yang, R. Liang, W. Shi and H. C. Zhou, *Chem. Rev.*, 2023, **123**, 5347–5420.
2 J. Rittle and M. T. Green, *Science*, 2021, **330**, 933–937.
3 R. H. Holm and E. I. Solomon, *Chem. Rev.*, 2014, **114**, 3367–3368.
4 M. W. Grinstaff, M. G. Hill, J. A. Labinger and H. B. Gray, *Science*, 1994, **264**, 1311–1313.
5 C. J. Hastings, M. D. Pluth, R. G. Bergman and K. N. Raymond, *J. Am. Chem. Soc.*, 2010, **132**, 6938–6940.
6 D. M. Vriezema, M. Comellas Aragonès, J. A. A. W. Elemans, J. J. L. M. Cornelissen, A. E. Rowan and R. J. M. Nolte, *Chem. Rev.*, 2005, **105**, 1445–1490.
7 Z. Dong, Q. Luo and J. Liu, *Chem. Soc. Rev.*, 2012, **41**, 7890–7908.
8 D. H. Qu, Q. C. Wang, Q. W. Zhang, X. Ma and H. Tian, *Chem. Rev.*, 2015, **115**, 7543–7588.
9 https://www.nobelprize.org/prizes/chemistry/1987/summary/.
10 https://www.nobelprize.org/prizes/chemistry/2016/summary/.
11 G. Crini, *Chem. Rev.*, 2014, **114**, 10940–10975.
12 Z. Liu, S. K. M. Nalluri and J. F. Stoddart, *Chem. Soc. Rev.*, 2017, **46**, 2459–2478.
13 G. Sachdeva, D. Vaya, C. M. Srivastava, A. Kumar, V. Rawat, M. Singh, M. Verma, P. Rawat and G. K. Rao, *Coord. Chem. Rev.*, 2022, **472**, 214791.
14 J. Lagona, P. Mukhopadhyay, S. Chakrabarti and L. Isaacs, *Angew. Chem., Int. Ed.*, 2005, **44**, 4844–4870.
15 S. Yue, Y. Zhou, Y. Yao and M. Xue, *Acta Chim. Sin.*, 2014, **72**, 1053.
16 S. Hiroto, Y. Miyake and H. Shinokubo, *Chem. Rev.*, 2017, **117**, 2910–3043.
17 G. Zhang and M. Mastalerz, *Chem. Soc. Rev.*, 2014, **43**, 1934–1947.
18 J. R. Li and H. C. Zhou, *Nat. Chem.*, 2010, **2**, 893–898.
19 T. Skorjanc, D. Shetty and A. Trabolsi, *Chem*, 2021, **7**, 882–918.
20 A. Ovsyannikov, S. Solovieva, I. Antipin and S. Ferlay, *Coord. Chem. Rev.*, 2017, **352**, 151–186.
21 M. A. Little and A. I. Cooper, *Adv. Funct. Mater.*, 2020, **30**, 1909842.
22 Y. Liang, E. Li, K. Wang, Z. J. Guan, H. He, L. Zhang, H. C. Zhou, F. Huang and Y. Fang, *Chem. Soc. Rev.*, 2022, **51**, 8378–8405.
23 X. Ji, H. Wang, H. Wang, T. Zhao, Z. A. Page, N. M. Khashab and J. L. Sessler, *Angew. Chem., Int. Ed.*, 2020, **59**, 23402–23412.
24 H. Wang, Y. Jin, N. Sun, W. Zhang and J. Jiang, *Chem. Soc. Rev.*, 2021, **50**, 8874–8886.
25 J. Liang, A. Nuhnen, S. Millan, H. Breitzke, V. Gvilava, G. Buntkowsky and C. Janiak, *Angew. Chem., Int. Ed.*, 2020, **59**, 6068–6073.
26 L. Chen, R. Luque and Y. Li, *Chem. Soc. Rev.*, 2017, **46**, 4614–4630.
27 X. T. Liu, B. B. Qian, D. S. Zhang, M. H. Yu, Z. Chang and X. H. Bu, *Coord. Chem. Rev.*, 2023, **476**, 214921.
28 Y. Cui, Y. Zhao, J. Wu and H. Hou, *Nano Today*, 2023, **52**, 101972.
29 H. C. Zhou and S. Kitagawa, *Chem. Soc. Rev.*, 2014, **43**, 5415–5418.
30 R. Freund, O. Zaremba, G. Arnauts, R. Ameloot, G. Skorupskii, M. Dincă, A. Bavykina, J. Gascon, A. Ejsmont, J. Goscianska, M. Kalmutzki, U. Lächelt, E. Ploetz, C. S. Diercks and S. Wuttke, *Angew. Chem., Int. Ed.*, 2021, **60**, 23975–24001.
31 H. Furukawa, K. E. Cordova, M. O'Keeffe and O. M. Yaghi, *Science*, 2013, **341**, 1230444.

32 H. Y. Guan, R. J. LeBlanc, S. Y. Xie and Y. Yue, *Coord. Chem. Rev.*, 2018, **369**, 76–90.
33 G. Férey, C. Mellot–Draznieks, C. Serre, F. Millange, J. Dutour, S. Surblé and I. Margiolaki, *Science*, 2005, **309**, 2040–2042.
34 X. Qiu, W. Zhong, C. Bai and Y. Li, *J. Am. Chem. Soc.*, 2016, **138**, 1138–1141.
35 S. M. Cohen, *Chem. Rev.*, 2012, **112**, 970–1000.
36 J. P. Zhang, Y. B. Zhang, J. B. Lin and X. M. Chen, *Chem. Rev.*, 2012, **112**, 1001–1033.
37 M. Ding, X. Cai and H. L. Jiang, *Chem. Sci.*, 2019, **10**, 10209–10230.
38 S. Furukawa, J. Reboul, S. Diring, K. Sumida and S. Kitagawa, *Chem. Soc. Rev.*, 2014, **43**, 5700–5734.
39 J. Liang, V. Gvilava, C. Jansen, S. Ozturk, A. Spiess, J. Lin, S. Xing, Y. Sun, H. Wang and C. Janiak, *Angew. Chem., Int. Ed.*, 2021, **60**, 15365–15370.
40 Y. Ban, Z. Li, Y. Li, Y. Peng, H. Jin, W. Jiao, A. Guo, P. Wang, Q. Yang, C. Zhong and W. Yang, *Angew. Chem., Int. Ed.*, 2015, **54**, 15483–15487.
41 D. Y. Du, J. S. Qin, S. L. Li, Z. M. Su and Y. Q. Lan, *Chem. Soc. Rev.*, 2014, **43**, 4615–4632.
42 S. Huang, G. Chen and G. Ouyang, *Chem. Soc. Rev.*, 2022, **51**, 6824–6863.
43 W. Y. Gao, M. Chrzanowski and S. Ma, *Chem. Soc. Rev.*, 2014, **43**, 5841–5866.
44 M. H. Alkordi, Y. Liu, R. W. Larsen, J. F. Eubank and M. Eddaoudi, *J. Am. Chem. Soc.*, 2008, **130**, 12639–12641.
45 D. Masih, V. Chernikova, O. Shekhah, M. Eddaoudi and O. F. Mohammed, *ACS Appl. Mater. Interfaces*, 2018, **10**, 11399–11405.
46 R. W. Larsen, L. Wojtas, J. Perman, R. L. Musselman, M. J. Zaworotko and C. M. Vetromile, *J. Am. Chem. Soc.*, 2011, **133**, 10356–10359.
47 Z. Zhang, L. Zhang, L. Wojtas, M. Eddaoudi and M. J. Zaworotko, *J. Am. Chem. Soc.*, 2012, **134**, 928–933.
48 Z. Zhang, L. Zhang, L. Wojtas, P. Nugent, M. Eddaoudi and M. J. Zaworotko, *J. Am. Chem. Soc.*, 2012, **134**, 924–927.
49 Z. Zhang, W.-Y. Gao, L. Wojtas, S. Ma, M. Eddaoudi and M. J. Zaworotko, *Angew. Chem., Int. Ed.*, 2012, **51**, 9330–9334.
50 H. He, Q. Q. Zhu, C. Zhang, Y. Yan, J. Yuan, J. Chen, C. P. Li and M. Du, *Chem. – Asian J.*, 2019, **14**, 958–962.
51 N. Sharma, S. S. Dhankhar and C. M. Nagaraja, *Sustainable Energy Fuels*, 2019, **3**, 2977–2982.
52 P. Ling, J. Lei, L. Zhang and H. Ju, *Anal. Chem.*, 2015, **87**, 3957–3963.
53 A. B. Sorokin, *Chem. Rev.*, 2013, **113**, 8152–8191.
54 E. Kockrick, T. Lescouet, E. V. Kudrik, A. B. Sorokin and D. Farrusseng, *Chem. Commun.*, 2011, **47**, 1562–1564.
55 B. Li, Y. Zhang, D. Ma, T. Ma, Z. Shi and S. Ma, *J. Am. Chem. Soc.*, 2014, **136**, 1202–1205.
56 M. B. Boroujeni, A. Hashemzadeh, A. Shaabani and M. M. Amini, *Appl. Organomet. Chem.*, 2017, **31**, e3715.
57 A. D. Yeganeh, M. M. Amini and N. Safari, *J. Porphyrins phthalocyanines*, 2019, **23**, 1–14.
58 L. Ma, X. Han, S. Zhang, Z. Zeng, R. Song, X. Chen, D. Hou and L. Wang, *ACS Appl. Mater. Interfaces*, 2022, **14**, 13611–13621.
59 J. Li, Y. Shi, C. Qi, B. Zhang, X. Xing, Y. Li, T. Chen, X. Mao, Z. Zuo, X. Zhao, Z. Pan, L. Li, X. Yang and C. Li, *Angew. Chem., Int. Ed.*, 2023, **62**, e202309918.
60 T. Xu, B. Wu, W. Li, Y. Li, Y. Zhu, F. Sheng, Q. Li, L. Ge, X. Li, H. Wang and T. Xu, *Sci. Adv.*, 2024, **10**, eadn0944.
61 Z. Zhang, H. Zhu, H. Jin, Y. Cao, W. Fang, Z. Zhang, Q. Ma, J. Choi and Y. Li, *Angew. Chem., Int. Ed.*, 2024, e202415023.
62 V. I. Isaeva, O. P. Tkachenko, T. R. Brueva, G. I. Kapustin, E. V. Afonina, I. V. Mishin, V. Gryunert, L. M. Kustov, S. E. Solov'eva and I. S. Antipin, *Russ. J. Phys. Chem. A*, 2011, **85**, 293–297.
63 V. I. Isaeva, O. P. Tkachenko, E. V. Afonina, L. M. Kozlova, G. I. Kapustin, W. Grünert, S. E. Solov'eva, I. S. Antipin and L. M. Kustov, *Microporous Mesoporous Mater.*, 2013, **166**, 167–175.
64 I. Brekalo, C. M. Kane, A. N. Ley, J. R. Ramirez, T. Friščić and K. T. Holman, *J. Am. Chem. Soc.*, 2018, **140**, 10104–10108.
65 J. R. Ramirez, H. Yang, C. M. Kane, A. N. Ley and K. T. Holman, *J. Am. Chem. Soc.*, 2016, **138**, 12017–12020.
66 T. Hasell and A. I. Cooper, *Nat. Rev. Mater.*, 2016, **1**, 16053.
67 S. Funk and J. Schatz, *J. Inclusion Phenom. Macrocyclic Chem.*, 2020, **96**, 1–27.
68 Y. Huang, R. H. Gao, M. Liu, L. X. Chen, X. L. Ni, X. Xiao, H. Cong, Q. J. Zhu, K. Chen and Z. Tao, *Angew. Chem., Int. Ed.*, 2020, **60**, 15166–15191.
69 X. L. Ni, X. Xiao, H. Cong, L. L. Liang, K. Cheng, X. J. Cheng, N. N. Ji, Q. J. Zhu, S. F. Xue and Z. Tao, *Chem. Soc. Rev.*, 2013, **42**, 9480–9508.
70 Y. Sun, J. Liang, P. Brandt, A. Spieß, S. Öztürk and C. Janiak, *Nanoscale*, 2021, **13**, 15952–15962.
71 R. Ham, C. J. Nielsen, S. Pullen and J. N. H. Reek, *Chem. Rev.*, 2023, **123**, 5225–5261.
72 B. C. Wang, Z. Y. Feng, B. B. Hao, C. X. Zhang and Q. L. Wang, *Chem. – Eur. J.*, 2021, **27**, 12137–12143.
73 J. Lee, D. W. Lim, S. Dekura, H. Kitagawa and W. Choe, *ACS Appl. Mater. Interfaces*, 2019, **11**, 12639–12646.
74 S. Fajal, W. Mandal, S. Mollick, Y. D. More, A. Torris, S. Saurabh, M. M. Shirolkar and S. K. Ghosh, *Angew. Chem., Int. Ed.*, 2022, **61**, e202203385.
75 T. J. Pisklak, M. Macías, D. H. Coutinho, R. S. Huang and K. J. Balkus, *Top. Catal.*, 2006, **38**, 269–278.
76 V. Lykourinou, Y. Chen, X. S. Wang, L. Meng, T. Hoang, L. J. Ming, R. L. Musselman and S. Ma, *J. Am. Chem. Soc.*, 2011, **133**, 10382–10385.
77 Y. Chen, V. Lykourinou, C. Vetromile, T. Hoang, L. J. Ming, R. W. Larsen and S. Ma, *J. Am. Chem. Soc.*, 2012, **134**, 13188–13191.
78 J. Navarro-Sánchez, N. Almora-Barrios, B. Lerma-Berlanga, J. J. Ruiz-Pernía, V. A. Lorenz-Fonfria, I. Tunón and C. Martí-Gastaldo, *Chem. Sci.*, 2019, **10**, 4082–4088.
79 D. Feng, T. F. Liu, J. Su, M. Bosch, Z. Wei, W. Wan, D. Yuan, Y. P. Chen, X. Wang and K. Wang, *et al.*, *Nat. Commun.*, 2015, **6**, 5979.

80 P. Li, J. A. Modica, A. J. Howarth, E. Vargas L, P. Z. Moghadam, R. Q. Snurr, M. Mrksich, J. T. Hupp and O. K. Farha, *Chem*, 2016, **1**, 154–169.
81 X. Lian, Y. P. Chen, T. F. Liu and H. C. Zhou, *Chem. Sci.*, 2016, **7**, 6969–6973.
82 K. Liang, C. J. Coghlan, S. G. Bell, C. Doonan and P. Falcaro, *Chem. Commun.*, 2016, **52**, 473–476.
83 F. Lyu, Y. Zhang, R. N. Zare, J. Ge and Z. Liu, *Nano Lett.*, 2014, **14**, 5761–5765.
84 W. Liang, H. Xu, F. Carraro, N. K. Maddigan, Q. Li, S. G. Bell, D. M. Huang, A. Tarzia, M. B. Solomon and H. Amenitsch, *et al.*, *J. Am. Chem. Soc.*, 2019, **141**, 2348–2355.
85 Y. M. Li, J. Yuan, H. Ren, C. Y. Ji, Y. Tao, Y. Wu, L. Y. Chou, Y. B. Zhang and L. Cheng, *J. Am. Chem. Soc.*, 2021, **143**, 15378–15390.
86 H. An, J. Song, T. Wang, N. Xiao, Z. Zhang, P. Cheng, S. Ma, H. Huang and Y. Chen, *Angew. Chem., Int. Ed.*, 2020, **59**, 16764.
87 Y. Zhong, L. Yu, Q. He, Q. Zhu, C. Zhang, X. Cui, J. Zheng and S. Zhao, *ACS Appl. Mater. Interfaces*, 2019, **11**, 32769–32777.
88 L. Qi, Z. Luo and X. Lu, *ACS Sustainable Chem. Eng.*, 2019, **7**, 7127–7139.
89 K. Liang, R. Ricco, C. M. Doherty, M. J. Styles, S. Bell, N. Kirby, S. Mudie, D. Haylock, A. J. Hill and C. J. Doonan, *et al.*, *Nat. Commun.*, 2015, **6**, 7240.
90 F. K. Shieh, S. C. Wang, C. I. Yen, C. C. Wu, S. Dutta, L. Y. Chou, J. V. Morabito, P. Hu, M. H. Hsu and K. C. W. Wu, *et al.*, *J. Am. Chem. Soc.*, 2015, **137**, 4276–4279.
91 S. Y. Chen, W. S. Lo, Y. D. Huang, X. Si, F. S. Liao, S. W. Lin, B. P. Williams, T. Q. Sun, H. W. Lin and Y. An, *et al.*, *Nano Lett.*, 2020, **20**, 6630–6635.
92 W. Liang, P. Wied, F. Carraro, C. J. Sumby, B. Nidetzky, C. K. Tsung, P. Falcaro and C. J. Doonan, *Chem. Rev.*, 2021, **121**, 1077–1129.
93 X. Zhang, R. Tu, Z. Lu, J. Peng, C. Hou and Z. Wang, *Coord. Chem. Rev.*, 2021, **443**, 214032.
94 C. Wang and K. Liao, *ACS Appl. Mater. Interfaces*, 2021, **13**, 56752–56776.
95 R. J. Drout, L. Robison and O. K. Farha, *Coord. Chem. Rev.*, 2019, **381**, 151–160.
96 W. Chen, Y. Tan, H. Zheng, Z. Wang, Z. Qu and C. Wu, *Microchem. J.*, 2024, **206**, 111441.
97 E. Barea, C. Montoro and J. A. Navarro, *Chem. Soc. Rev.*, 2014, **43**, 5419–5430.
98 Z. Zhang, Z. Z. Yao, S. Xiang and B. Chen, *Energy Environ. Sci.*, 2014, **7**, 2868–2899.
99 J. Liang, S. Xing, P. Brandt, A. Nuhnen, C. Schlüsener, Y. Sun and C. Janiak, *J. Mater. Chem. A*, 2020, **8**, 19799–19804.
100 S. Xing, J. Liang, P. Brandt, F. Schäfer, A. Nuhnen, T. Heinen, I. Boldog, J. Möllmer, M. Lange, O. Weingart and C. Janiak, *Angew. Chem., Int. Ed.*, 2021, **60**, 17998–18005.
101 S. Bolisetty, M. Peydayesh and R. Mezzenga, *Chem. Soc. Rev.*, 2019, **48**, 463–487.
102 J. Li, X. Wang, G. Zhao, C. Chen, Z. Chai, A. Alsaedi, T. Hayat and X. Wang, *Chem. Soc. Rev.*, 2018, **47**, 2322–2356.
103 L. Zou, R. Sa, H. Lv, H. Zhong and R. Wang, *ChemSusChem*, 2020, **13**, 6124–6140.
104 P. Li, S. Y. Moon, M. A. Guelta, S. P. Harvey, J. T. Hupp and O. K. Farha, *J. Am. Chem. Soc.*, 2016, **138**, 8052–8055.
105 L. Wang, W. Zhi, J. Wan, J. Han, C. Li and Y. Wang, *ACS Sustainable Chem. Eng.*, 2019, **7**, 3339–3348.
106 G. Chen, X. Kou, S. Huang, L. Tong, Y. Shen, W. Zhu, F. Zhu and G. Ouyang, *Angew. Chem., Int. Ed.*, 2020, **59**, 2867–2874.
107 X. Wu, J. Ge, C. Yang, M. Hou and Z. Liu, *Chem. Commun.*, 2015, **51**, 13408–13411.
108 J. Zhou, S. Yu, H. Kang, R. He, Y. Ning, Y. Yu, M. Wang and B. Chen, *Renew. Energy*, 2020, **156**, 107–116.
109 Y. Li, L. Wen, T. Tan and Y. Lv, *Front. Bioeng. Biotechnol.*, 2019, **7**, 394.
110 Q. Zhang, L. Zhang, H. Dai, Z. Li, Y. Fu and Y. Li, *J. Electroanal. Chem.*, 2018, **823**, 40–46.
111 G. Zhu, M. Zhang, L. Lu, X. Lou, M. Dong and L. Zhu, *Sens. Actuators, B*, 2019, **288**, 12–19.
112 J. Song, W. He, H. Shen, Z. Zhou, M. Li, P. Su and Y. Yang, *Chem. Eng. J.*, 2019, **363**, 174–182.
113 Y. Xu, S.-Y. Liu, J. Liu, L. Zhang, D. Chen, J. Chen, Y. Ma, J.-P. Zhang, Z. Dai and X. Zou, *Chem. – Eur. J.*, 2019, **25**, 5463–5471.
114 B. Wang, Y. Luo, L. Gao, B. Liu and G. Duan, *Biosens. Bioelectron.*, 2021, **171**, 112736.
115 X. Kou, L. Tong, Y. Shen, W. Zhu, L. Yin, S. Huang, F. Zhu, G. Chen and G. Ouyang, *Biosens. Bioelectron.*, 2020, **156**, 112095.
116 S. Wu, Z. Sun, Y. Peng, Y. Han, J. Li, S. Zhu, Y. Yin and G. Li, *Biosens. Bioelectron.*, 2020, **169**, 112613.
117 X. Zhong, F. Wang, J. Piao and Y. Chen, *Analyst*, 2021, **146**, 2825–2833.
118 Z. Ji, B. Zhou, Z. Shang, S. Liu, X. Li, X. Zhang and B. Li, *Anal. Chem.*, 2023, **95**, 10580–10587.
119 G. Yu, X. Yan, C. Han and F. Huang, *Chem. Soc. Rev.*, 2013, **42**, 6697–6722.
120 J. Liang, Y. Q. Xie, Q. Wu, X. Y. Wang, T. T. Liu, H. F. Li, Y. B. Huang and R. Cao, *Inorg. Chem.*, 2018, **57**, 2584–2593.
121 M. Zhao, K. Yuan, Y. Wang, G. Li, J. Guo, L. Gu, W. Hu, H. Zhao and Z. Tang, *Nature*, 2016, **539**, 76–80.
122 A. Nuhnen and C. Janiak, *Dalton Trans.*, 2020, **49**, 10295–10307.
123 T. Kitao, Y. Zhang, S. Kitagawa, B. Wang and T. Uemura, *Chem. Soc. Rev.*, 2017, **46**, 3108–3133.
124 J. Y. Li, X. D. Yang, F. X. Chen and J. K. Sun, *Mater. Chem. Front.*, 2023, **7**, 5355–5376.

